THE UNIVERSITY OF CHICAGO

The Effects of Propofol on Hurst Exponent During Rest and Narrative Listening

By

Mianzhi Hu

April 2023

A paper submitted in partial fulfillment of the requirements for the Master of Arts degree in the Master of Arts Program in the Social Sciences

Faculty Advisor: Marc Berman

Preceptor: Hannah Hamilton

Abstract

The current study utilized a rarely used statistical tool in anesthetic research, Hurst analysis, to a group of participants who received propofol administration. Our results suggest that the visual imagery pathway, involving visual attention, primary and secondary visual cortex, is the primary target for propofol modulation during sedation. The moving window approach revealed qualitative differences in the brain activity within a single scanning session, which has not been reported in the literature. Together, our findings add to the emerging literature on the dissociation between mental imagery abilities and consciousness and provide evidence for visual imagery processing in behaviorally unresponsive participants.

The Effects of Propofol on Hurst Exponent During Rest and Narrative Listening

Studying reduced levels of consciousness can unveil the pharmaceutical mechanisms of sedative drugs and elucidate brain functioning under various states. However, despite existing efforts, much remains unclear about the sedated brain, particularly the neural processes that occur during the waning of consciousness (Hudetz, 2012; Kandeepan et al., 2020). As such, the present study applied Hurst analysis, a statistical tool rarely used in anesthetic research, to analyze functional magnetic resonance imaging (fMRI) data from sedated participants and explore the selective modulation of the brain by propofol (Hurst, 1951; Kardan et al., 2020). Our aim is to conduct an in-depth examination of the impact of propofol on the Hurst exponent (*H*) in the brain across time and space, with the ultimate goal of providing a unique perspective to understand the effects of propofol and contributing to the growing body of knowledge on sedative drugs and brain functioning.

Hurst analysis is a statistical tool that has shown promise in evaluating the fractalness of time series data (i.e., how similar does a signal look at different timescales). It has been successfully applied in various modalities, including fMRI, electroencephalography (EEG), and functional near-infrared spectroscopy (fNIRS; Ciuciu et al., 2012; Kardan et al., 2020; Zhuang et al., 2022), but largely overlooked in the research of brain functioning under anesthesia. To date, Varley et al. (2020) was the only study that employed Hurst analysis to analyze neuroimaging data from sedated participants. They found that *H* was generally higher, indicating a reduction in overall brain activity, during sedation compared to wakefulness.

The framework of Hurst analysis is built upon the concept of fractal, which refers to the mathematical object that displays scale invariance (Churchill et al., 2014; Kardan et al., 2020; Stier et al., 2021). A higher Hurst exponent, *H*, denotes greater structural self-similarity at

different levels of magnification or across different timescales (see *Figure 1*). In psychology, *H* has been associated with many cognitive and affective processes, such as learning, task difficulty, and psychopathology (Churchill et al., 2016; Kardan et al., 2020; Stier et al., 2021; Wei et al., 2013). Multiple studies have suggested that *H* is a computationally efficient index for assessing cognitive resource allocation. A decreased regional *H* typically represents more mental effort, or more cognitive resources allocated to the corresponding brain region (Churchill et al., 2016; Kardan et al., 2020; Stier et al., 2021). Individuals generally exhibit lower *H* values during tasks as compared to the resting state (He, 2011; Kardan et al., 2020). Novel and complex tasks can induce a further decrease in regional *H* values as people exert more efforts to learn and integrate the rules and suppress irrelevant information. A higher *H* has been found to separate good task-learners from mediocre ones potentially because the former has developed helpful task-related memories and effective cognitive strategies to make the same task less resource-consuming (Churchill et al., 2016; Kardan et al., 2020).

Figure 1

Example Hurst time series

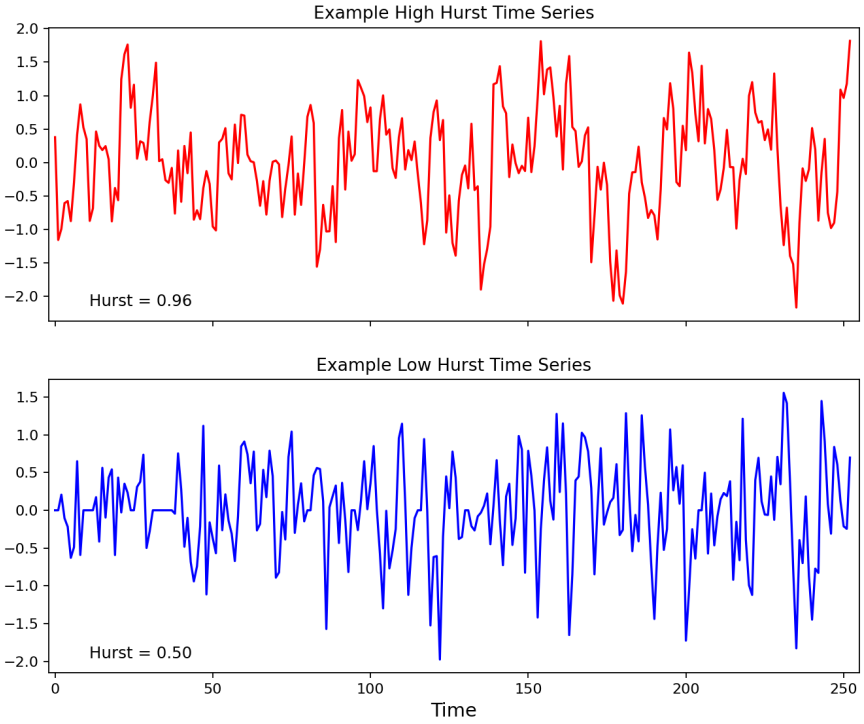

Note. H close to 1 would have smoother looking temporal fluctuations (top) while *H* close to 0.5 looks like random noise (bottom). The top signal can be described as more fractal, or, more self-similar than the bottom signal.

The critical state theory was proposed to account for the relationship between *H* and cognitive processes. In physics, a critical state is a state of a system that is poised at a phase transition point and ready to undergo a sudden and large-scale reorganization in response to environmental changes (Cocchi et al., 2017). In the brain, the critical state allows optimal information transmission and adaptability by maximizing the potential information exchange between different brain systems (Cocchi et al., 2017). In other words, the brain at criticality is readily transformable to any task-relevant states depending on external demands. Researchers have suggested that *H* could serve as a real-time index of how close the brain is to a critical state,

with higher *H* (close to 1) values indicating greater proximity to the critical state (Cocchi et al., 2017; Kardan et al., 2020; Stier et al., 2021). As the task demand increases, the information exchange between relevant brain regions is strengthened to adapt to the task. Consequently, the cognitive resource allocation becomes less flexible, and the brain moves away from the critical state, leading to a decreased *H* (Cocchi et al., 2017; Kardan et al., 2020).

Given the fruitful results generated by Hurst analysis in other domains of psychology and neuroscience, this method deserves further attention in the realm of anesthesia research for at least three reasons. First, it is capable of uncovering hidden patterns in neuroimaging data that may have been missed by other techniques. For instance, previous studies investigating neural activity during sleep have reported a decrease of *H* during later stages of sleep, potentially indicating an increase of brain activity. (Acharya et al., 2005; Song et al., 2007; Sriraam et al., 2014). Specifically, Song et al. (2007) identified a periodic inverted U-shape fluctuation of *H* in which *H* peaked during slow wave sleep and dropped as participants moved to the rapid eye movement (REM) sleep stage. In contrast, current models of propofol-induced sedation typically assume a linear degradation of cognitive functions (Davis et al, 2007; Gross et al., 2019). Given the evidence of partially shared neural mechanisms underlying sleep and sedation, Hurst analysis applied to the sedated brain may complement our knowledge in terms of the temporal trend of sedative effects (Franks & Wisden, 2021; Hall et al., 2014). Second, *H*, as a transdiagnostic and trans-state index for cognitive resource allocation, facilitates cross-state comparisons (e.g., sedation and sleep). Such comparisons help illuminate the shared neural mechanisms underlying seemingly distinct cognitive processes, which could lead to the development of more effective pharmaceutical interventions and psychological treatments. Finally, rather than treating each scanning session as a single, uniform event, Hurst analysis allows for the selection of different

window sizes and the iteration through partially overlapping windows, making it possible to capture subtle temporal dynamics within a single scanning session. While other tools, such as functional connectivity analysis, may also be used for this purpose, they are still in their early stages and provide only "coarse-grained approximations" (Bassett et al., 2018). Hurst analysis, as deeply rooted in the literature of criticality, comes with a well-developed mathematical toolset which offers robust models for precise quantification of such micro temporal fractals (Stier et al., 2021). This is particularly insightful in the research of anesthetics because the sedative agent takes effect gradually. Moreover, participants may be asked to verbally respond to questions before the scanning session begins (Naci et al., 2018; Kandeepan et al., 2020). The process of returning to the baseline also takes time and might vary depending on the sedation level. Thus, by delineating detailed temporal patterns, Hurst analysis provides a more refined and nuanced picture of the interactions between the brain and the agent (Stier et al., 2021).

Despite the limited application of Hurst analysis in current anesthetic research, what can we learn about propofol and the sedated brain from existing literature? Propofol is a widely used short-acting anesthetic agent. Following administration, it is quickly metabolized by the liver into inactive, water-soluble compounds, which are then eliminated by the kidneys, allowing subjects to be promptly woken after discontinuation (Tobias & Leder, 2011). Its rapid onset, rapid recovery time, and absence of active metabolites make it a popular choice for both procedural sedation and neuroscience research. Prior research has demonstrated that propofol can cause substantial impairments to cognitive abilities such as speech comprehension, verbal communication, and memory, and lead to a prolonged response time to both auditory and visual stimuli (Davis et al., 2007; Kandeepan et al., 2020; Kim et al., 2004; Veselis et al., 1992). These impairments are often associated with detectable activity changes in the relevant brain regions.

For instance, Davis et al. (2007) observed greater inferior frontal and posterior temporal blood-oxygen-level-dependent (BOLD) responses to ambiguous sentences compared to clear sentences when the participants were fully conscious. The additional activity vanished during propofol-induced sedation, which may reflect deficits in complex verbal comprehension. Likewise, voice-specific and word-specific activations in the temporal lobe were found to be abolished during propofol-induced sedation and scrambled words elicited more activations bilaterally than normal words. Although the primary and association auditory cortex remained responsive to auditory stimuli, the non-specificity suggests a loss of higher-level semantic processing (Plourde et al., 2006). Dueck et al. (2005) also reported dose-dependent impairments in auditory information processing after propofol administration. Although the superior temporal gyrus continued to actively process basic acoustic information even at the highest dose, activation in higher-order processing areas such as the precentral gyrus, inferior frontal gyrus, and insula were immediately inhibited following propofol administration.

Neuroimaging studies on the visual system are relatively scarce in anesthetics research, potentially due to challenges in keeping participants' eyes open during deep sedation. Nevertheless, available research on propofol and similar sedatives shows that the effects on the visual system are comparable to those observed in the auditory system. During sedation, activities in higher-order association cortices tend to be attenuated, resulting in a sluggish response to visual stimuli and partial amnesia for complex visual scenes (Hudetz, 2012; Kim et al., 2004; Veselis et al., 1992). Visual-evoked potentials (VEP) show lower amplitude, lower frequency, and slower waves with low doses of propofol, and exhibit burst suppression with high doses (Aggarwal et al., 2019; Hamaguchi et al., 2005). In addition, cross-modal interactions diminish during propofol-induced sedation, likely because of deactivation in the association

cortices of sensory systems. Boveroux et al. (2010) identified a negative correlation between thalamocortical activity and cortical activity in frontoparietal networks during sedation. Specifically, sensory processing in visual and auditory networks were preserved at thalamocortical level but the resulting information was inhibited from being transmitted and synthesized in the frontal areas. Taken together, these findings suggest that the frontoparietal cortex is the major target of propofol. Higher-order cognitive networks located around this area are less engaged in sensory stimulus processing during propofol-induced sedation, whereas primary sensory cortices remain at least partially responsive, even at the deepest sedative level (Davis et al., 2007; Hudetz, 2012; Kandeepan et al., 2020; Plourde et al., 2006).

In the present study, our dataset includes two conditions, narrative listening and resting, and four sedation levels (awake, mild sedation, deep sedation, and recovery). We started by comparing whole-brain *H* across conditions and sedation levels, where whole-brain *H* was the average of all regional *H* values across the brain. Next, we conducted partial least squares (PLS) analysis to identify the latent variable that captures the unique effect of propofol. We then examined the significant brain nodes for the latent variable and evaluated the spatial correlation between the latent variable and Neurosynth terms. To identify the brain networks with the most significant brain loadings, we applied the brain mask developed by Shen et al. (2013). Finally, we employed a smaller window size and a moving window approach to delineate the fine-grained temporal dynamics of *H* within each scanning session. By taking these steps, we were able to identify an inverted-U shape relationship between whole-brain *H* and sedation level in the narrative listening condition. We also found evidence for the occurrence of unconscious mental imagery processes during later stages of sedation. Surprisingly, our analyses did not reveal any modulation of auditory areas by propofol, contradictory to some previous studies.

Method

Dataset

We conducted secondary analyses of data sourced from Openneuro.org, which is accessible via the link (https://openneuro.org/datasets/ds003171/versions/2.0.1) and has been used in previous studies (Chamberlain & Rosenberg, 2022; Kandeepan et al. 2020; Naci et al. 2018). The fMRI data were collected while participants were at rest and while the same participants were listening to a 5:12-minute audio excerpt from the movie "Taken" at four different levels of propofol-induced sedation.

Participants

The study was conducted at Western University and was granted ethical approval by the Health Sciences Research Ethics Board and Psychology Research Ethics Board of Western University (REB #104755). A total of 17 subjects (4 women; mean age: 24 years, SD = 5) were recruited for the study. All participants were right-handed, native English speakers, and had no history of neurological disorders. Recruitment was done through printed advertisements on the university campus and through word of mouth. Volunteers completed a magnetic resonance imaging (MRI) and propofol safety screening and provided written informed consent to confirm that they understood study risks and had no contraindications for MRI or sedation. Participants were paid for their participation (Kandeepan et al., 2020).

Task Protocol

FMRI scans were collected from the 17 participants in four distinct states of consciousness: awake, mild sedation, deep sedation, and recovery. During each sedation level, narrative listening and resting-state scans were obtained (5 min and 8 min, respectively). For

each sedation level, the narrative listening scans always preceded resting scans once the sedation level was determined (See *Figure 2*). During the 5-min narrative listening scan, participants listened to an audio excerpt from the movie "Taken" with their eyes closed. The audio story was selected due to its emotional evocation and high arousal levels (Kandeepan et al., 2020). Specifically, the clip portrays a teenage girl being kidnapped while speaking to her father on the phone (Naci et al., 2018). During the subsequent 8-min resting scan, participants were instructed to relax with their eyes closed without falling asleep.

Propofol Administration

According to Kandeepan et al. (2020), participants received intravenous propofol before the fMRI scanning session. A 20 G intravenous cannula was inserted into the dorsum of the non-dominant hand prior to entering the scanner, and the propofol infusion system was connected to the cannula. An effect-site/plasma steering algorithm was used with the computer-controlled infusion pump to achieve stepwise increments in the sedative effect of propofol. The infusion pump was adjusted to reach the desired level of sedation, based on targeted concentrations of propofol predicted by the TIVATrainer pharmacokinetic simulation program. The estimated mean effect-site and plasma propofol concentrations were 2.48 (1.82–3.14) μg/ml and 2.68 (1.92–3.44) μg/ml, respectively, with a mean total mass of propofol administered of 486.58 (373.30–599.86) mg.

Sedation Assessment

The assessment of sedation level was based on the Ramsay level, which classifies a person's level of sedation on a scale from 1 (severe agitation) to 6 (deep coma). Two anesthesiologists and one anesthesia nurse independently evaluated each participant's Ramsay

level by communicating with them inside the fMRI scanner room before data acquisition. Scanning began only after an agreement was reached among the three assessors on the participant's wakefulness/sedation level.

The awake session involved no administration of propofol, and participants were fully awake, alert, and communicating appropriately. For the mild sedation session, propofol infusion began with a target effect-site concentration of 0.6 μg/ml, and participants were assessed for sedation level. Once they became calmer and less responsive to verbal communication, they were classified as a Ramsey level 3 and considered mildly sedated. Subsequently, the mild scanning session was performed. During the deep sedation session, the target effect-site concentration was increased incrementally until participants reached a Ramsey level 5, at which they were deeply sedated and no longer responsive to verbal commands. Propofol infusion was then discontinued, and participants reached a Ramsey level 2 approximately 11 minutes later during the recovery session, characterized by clear and quick responses to verbal commands. For further details on the propofol administration procedures, please refer to Naci et al. (2018) and Kandeepan et al. (2020).

Figure 2

Task Procedures

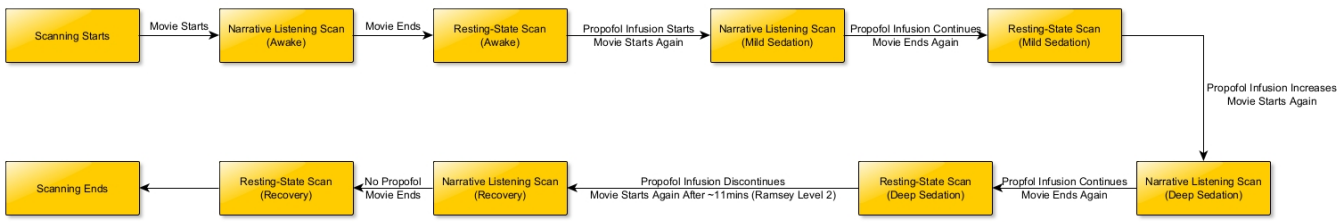

Note. This is an illustration of task procedures as implemented in the data collection process.

Participants went through awake, mild sedation, deep sedation, and recovery in a sequential order, with narrative listening scans always preceding resting-state scans.

FMRI Data Acquisition

The participants were provided with noise-canceling headphones during the MRI scan and the volume was adjusted to their comfort level (Naci et al., 2018). The MRI data were obtained using a 3-Tesla Siemens Tim Trio scanner with a 32-channel coil. The functional images were acquired with the following parameters – voxel size: 3×3×3 mm^3, inter-slice gap: 25%, time repetition (TR): 2,000 ms, time echo (TE): 30 ms, matrix size: 64×64, and flip angle (FA): 75°. The narrative scans and resting-state scans were collected with 155 and 256 volumes, respectively. Anatomical images were obtained with a T1-weighted 3D MPRAGE (Magnetization Prepared - Rapid Gradient Echo) sequence, using a 32-channel coil, with a voxel size of 1×1×1 mm^3, a TE of 4.25 ms, a matrix size of 240×256×192, and an FA of 9°.

FMRI Preprocessing

The fMRI data preprocessing pipeline utilized in this study was identical to the one described in Chamberlain & Rosenberg (2022) study. The data were preprocessed using Analysis of Functional NeuroImage (AFNI), and initial preprocessing steps included excluding the first three volumes, followed by despiking and head motion correction. Next, functional images were aligned with the skull-stripped anatomical image using linear transformation, then with the Montreal Neurological Institute atlas through nonlinear warping. To account for potential confounding variables, covariates such as the 24-parameter head motion model (6 motion parameters, 6 temporal derivatives, and their squares), subject-specific eroded white matter and ventricle masks, and the whole brain's mean signal were regressed from the data. Volumes in

which more than 10% of voxels were outliers, and volumes for which the Euclidean norm of the head motion parameter derivatives exceeded 0.25, were censored from the time series. Scans for which more than 50% of frames were censored for head motion were excluded from analyses. The BOLD signal time courses were averaged within regions of interest (ROI) using a 268-node whole-brain parcellation (Shen et al., 2013). Out of the 17 participants, 16 for awake, 15 for mild sedation, 11 for deep sedation, and 17 for recovery passed the motion exclusion for resting-state scans. For narrative-listening scans, 16 for awake, 15 for mild sedation, 11 for deep sedation, and 15 for recovery passed the motion exclusion. A total of 116 data files went into data analysis, containing partially overlapping participants.

Hurst Analysis

In the present study, two methods were employed for calculating *H*: detrended fluctuation analysis (DFA) and wavelet leader-based multifractal analysis (WLBMFA). Most of the analyses focused on *H* calculated with DFA, as it is generally recommended over wavelet approaches (Galaska et al., 2008; Oświęcimka et al., 2006; Zorick & Mandelkern, 2013). Although some evidence suggests that different methods for calculating *H* may generate comparable results (Kantelhardt et al., 2002), DFA has several advantages. For instance, it is known to be robust against noises and non-stationarity in the data, such as low-frequency drifts or high-frequency noise (Lee et al., 2002; López et al., 2021; Peng et al., 1995). In time series analysis, stationarity refers to the property of a stochastic process in which the statistical signatures (e.g., mean, variance, autocorrelation) of the process remain constant over time (Rhif et al., 2019). However, biological, physiological, and neuroimaging data are usually irregular and non-stationary (Lee et al., 2002; Peng et al., 1995). Whereas wavelet approaches typically handle non-stationarity by decomposing a time series into multiple frequency bands with different scales, DFA has been

found to be intrinsically robust against noises, such as missing data, random spikes, and varying standard deviations and correlations (Chen et al., 2002; Churchill et al., 2014; López et al., 2021; Robin et al., 2013). The simplicity of DFA calculation, combined with its natural robustness against non-stationarity, makes it computationally efficient (Churchill et al., 2014; Robin et al., 2013).

Moreover, wavelet approaches require the choice of several parameters (e.g., the wavelet basis function, block size, moment order range), adding a flavor of subjectivity in the results. Due to the lack of a clear consensus on the optimal parameter selection, variability can be introduced into the estimation of the multifractal properties (Rhif et al., 2019; Zorick & Mandelkern, 2013). Particularly in our case where the narrative listening session consisted of only about 150 volumes, decomposing the time series into multiple scales and blocks carries a heightened risk of overfitting and potentially insufficient data. Besides, DFA results can be easily interpreted in terms of the scaling properties of the time series data, such as the presence of long-range correlations or the degree of persistence. The singularity spectrum produced by the wavelet approaches provides a statistical description of the multifractal properties of the signal, but it may not be readily interpretable in terms of the underlying physical or biological mechanisms that generate the data. Hence, we relied mainly on DFA-based H in the current study and used WLBMFA as a means of validating DFA results.

Detrended Fluctuation Analysis

For each of the 268 shen-defined ROIs, in DFA, the time series $x(t)$ ($1 \leq t \leq T$) was transformed into an unbounded random walk by calculating the centered cumulative sum:

$$X(t) = \sum_{t=1}^{t} (x(i) - \bar{x})$$

(1)

Then, the detrended time series was partitioned into *N* non-overlapping windows of identical length *n*, where the product of *n* and *N* is less than or equal to the total number of time points in the data (*T*). To ensure minimal impact from confounding factors, we excluded any low-frequency confounds below 0.01 Hz and high-frequency confounds above 0.1 Hz, limiting the maximum *n* equal to 50 and the minimum to 5. For each window, a least squares linear regression *Y(t)* was fitted. By varying the window size *n*, the root mean square (RMS) fluctuation of the regression errors across all time series was computed as:

$$F(n) = \sqrt{\frac{\sum_{t=1}^{t}(X(t) - Y(t))^2}{N}}$$

(2)

Finally, *H* was obtained by determining the slope of a linear regression of the logarithm of the window size, *log(n)*, plotted against the logarithm of the fluctuation function, *log(F(n))*.

DFA is a "mono-fractal" analysis where a single exponent *H* is sufficient to fully describe the scaling relationship between local fluctuations and window size (Stier et al., 2021). Nonetheless, in real-world data, *H* may vary depending on the window size due to the presence of different scaling regimes or trends in the data that are not accounted for by the detrending process in DFA (Churchill et al., 2016; Stier et al., 2021). Also, for some individuals, their brain activity may not conform to a mono-fractal, linear relationship. As a result, it is crucial to evaluate the goodness of fit for the DFA regression line in order to identify any potential

confounding factors. To assess the goodness of fit, we utilized the coefficient of determination, R^2, calculated as:

$$R^2 = 1 - \frac{\sum\left(log(F(n)) - \widehat{log(F(n))}\right)^2}{\sum\left(log(F(n)) - \overline{log(F(n))}\right)^2} \quad (3)$$

Out of the 116 data files included in the DFA analysis, 14 had a mean R^2 lower than 0.9, indicating non-optimal goodness of fit (see *Supplementary Figure 1* for the distribution of R^2). To ensure the quality of our analysis, we removed these 14 files, which amounted to 12.07% of the total data. Therefore, all subsequent analyses involving DFA-based *H* values were based on the remaining 102 files.

Wavelet Leader-Based Multifractal Analysis

In the present study, the estimation of *H* using the WLBMFA approach was based on the methodology presented by Wendt et al. (2007). To ensure consistency with the original study, we retained all parameters, including vanishing moments, block size function, and mother wavelet.

Briefly, given a time series *x(t)* of length *T*, we first performed the discrete wavelet transformation (DWT) using Daubechies 6 as the mother-wavelet. The DWT decomposes the signal into multiple scales, each represented by an array of wavelet coefficients. Next, we computed the wavelet leaders for each scale *s*, defined as the maximum absolute wavelet coefficients within *N* non-overlapping blocks of size *n*. The wavelet leaders provide an efficient way to estimate the scaling behavior of the time series, as they are less sensitive to small-scale fluctuations than the wavelet coefficients. We estimated the structure function *S(q, s)* of the wavelet leaders at each scale *s* and for different orders of moments *q*, and then computed the

singularity spectrum *f(α)* using a Legendre transformation of the structure function, where α represents the local Hölder exponent characterizing the rate of change of the signal on different scales. Finally, we calculated the first-order log-cumulant C_1 by setting α to 1 and taking the derivative:

$$H = C_1 = f'(1) \quad (4)$$

In essence, by setting the local Hölder exponent to 1, the rate of change of the function is required to be globally bounded by a constant, which approximates the process of a mono-fractal analysis. As such, C_1 is a useful indicator of the average scaling properties of the signal across all time scales and serves as an equivalent to DFA-based *H* while taking account of multifractal properties. For a more comprehensive understanding of the statistical methods employed, we refer the reader to Wendt et al. (2007).

Partial Least Squares

PLS analysis was applied to identify the latent variable that represents the impact of propofol across four sedation levels. PLS is a multivariate data analysis technique that involves decomposing the covariance matrix between two mean-centered datasets. In the context of task-based mean-centered PLS, the observations in *X* are sorted according to the *N* experimental conditions, while *Y* is a dummy-coded matrix that represents the experimental groups or conditions (Krishnan et al., 2010). In our analysis, *X* represented the $n \times 268$ subject-by-parcellation matrix of *H*, and *Y* represented the $n \times 4$ subject-by-sedation-level matrix. By virtue of being mean-centered, the covariance matrix *X'Y* was subjected to singular value decomposition as:

$$X'Y = USV'$$

(5)

where U is the 268×4 matrix of left singular vectors (brain loadings), V is the 4×4 matrix of right singular vectors (propofol loadings), and S is the 4 by 1 diagonal matrix of singular value. The i^{th} column of U and V represent the loadings of the i^{th} latent variable. The proportion of crossblock covariance explained by the i^{th} latent variables is calculated as the ratio of the squared i^{th} singular value to the sum of all squared singular values. To assess the statistical significance of the PLS models, 10,000 permutations of the rows of the Hurst matrix X were performed, and the observed crossblock covariance was compared to permuted crossblock covariances. The stability of the left and right singular vectors was evaluated by 10,000 bootstrap resampling of both X and Y matrices. The bootstrap ratios were estimated by dividing the empirical loading by the bootstrap variance and were distributed normally under the null hypothesis. Only brain parcellations with an absolute bootstrap ratio higher than 3 were considered statistically significant.

Spatial Null Model

To accurately evaluate the statistical significance of the correlation between the latent variable representing propofol effects and Neurosynth terms, we employed spatial auto-correlation-preserving permutation tests known as "spin tests." The use of spin tests is necessary since traditional permutation tests that do not consider spatial autocorrelation can lead to an inflated rate of false positives (Burt et al., 2020). To generate null brain maps with preserved spatial autocorrelation, we utilized the BrainSMASH python package (https://brainsmash.readthedocs.io/en/latest/). BrainSMASH produces SA-preserving random maps that have variograms similar to the input brain map. Variograms are functions of spatial

distance *d* and measure the variance between all pairs of points that are a particular distance *d* apart. In our analysis, we used the Euclidean distance between the centroids of brain parcels.

Results

Briefly, this study conducted a secondary analysis of fMRI data collected from 17 healthy participants while listening to an audio excerpt from the movie "Taken" and while they were at rest at four different levels of propofol-induced sedation. The participants underwent awake, mild sedation, deep sedation, and recovery in a sequential order, with the narrative listening scan always preceding the resting-state scan. After preprocessing and head motion control, the fMRI data were parcellated into 268 predefined brain nodes (Shen et al., 2013). *H* was then computed for each brain node using both DFA and WLBMFA. Subsequent analyses were based on DFA results with a minimum R^2 of 0.9. The unique effect of propofol was quantified using PLS with 10,000 permutations and the stability was assessed with 10,000 bootstrap resampling of both X and Y matrices.

Whole-Brain Hurst - DFA

The whole-brain *H*, defined as the mean *H* across 268 brain nodes, was analyzed using mixed effect models with random intercepts. As depicted in *Figure 3*, the models revealed no significant main effect for either sedation level ($F(3, 87) = 0.38$, $p = .771$) or narrative listening ($F(1, 88) = 2.77$, $p = .100$). However, a significant interaction effect was observed ($F(3, 82) = 3.82$, $p = .013$). The quadratic relationship between sedation level and whole-brain *H* was contingent upon the experimental condition and only detected in the narrative listening condition ($t(82) = 2.75$, $p = .007$; *Figure 4*).

Figure 3

Whole-brain Hurst main effects of sedation level and narrative listening – DFA

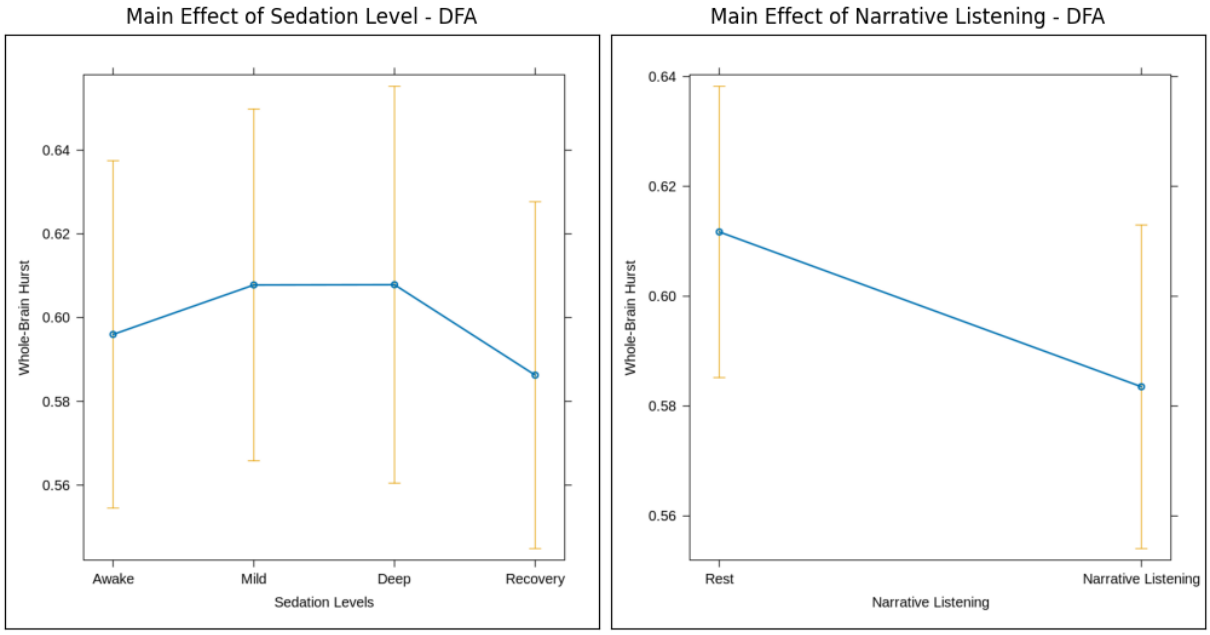

Note. Left: there was no significant main effect for sedation level ($F(3, 87) = 0.38$, $p = .771$). Right: There was not significant main effect for narrative listening either ($F(1, 88) = 2.77$, $p = .100$)

Figure 4

Whole-brain Hurst interaction effects – DFA

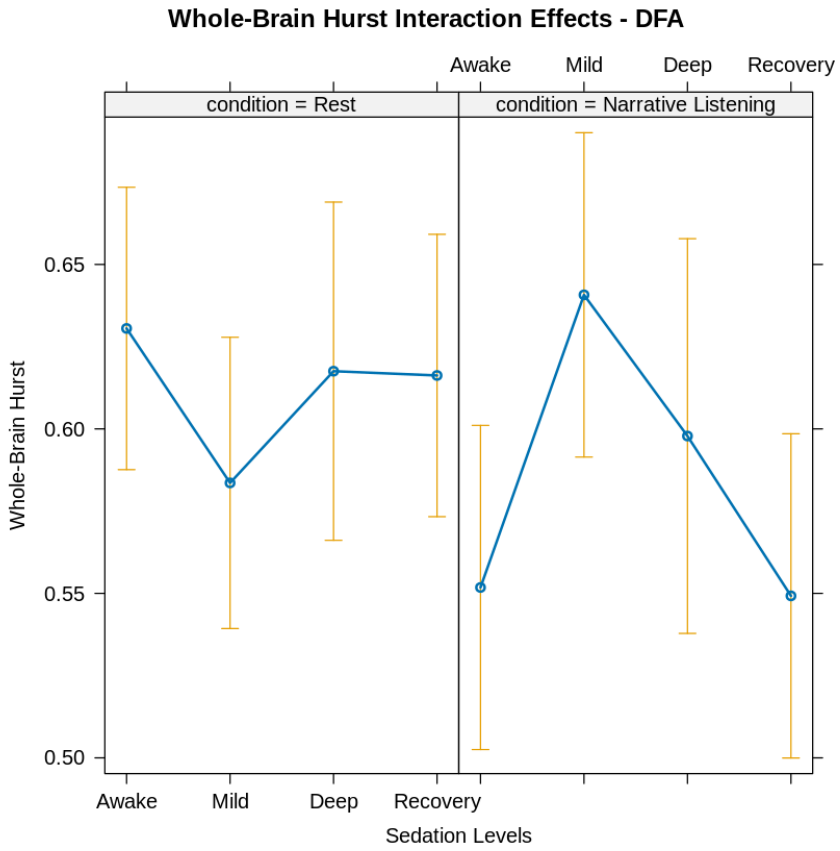

Note: In the resting condition (left), there were no significant interaction effects observed, whereas in the narrative listening condition (right), there was an increase in *H* from the awake to mild sedation level, followed by a peak at mild sedation, and a gradual return to baseline.

Whole-Brain Hurst - Wavelet

In addition to DFA, we also applied WLBMFA to assess the multifractal nature of the BOLD signal. This was done because the R^2 values obtained from DFA were not consistently high (> 0.9), which suggests that multifractal processes may be at play (see *Supplementary Figure 1*). Unsurprisingly, whole-brain *H* from WLBMFA and DFA had a strong positive correlation ($r(93) = .72$, $p < .001$) while WLBMFA-based *H* ($SD = 0.125$) showed greater variance than DFA-based *H* ($SD = 0.083$, $p = .004$). The instability of WLBMFA-based *H* is

supported by abundant statistical evidence indicating that wavelet approaches tend to yield greater overall variability compared to DFA (Kantelhardt et al., 2002; Oświęcimka et al., 2006; Zorick & Mandelkern, 2013). A linear regression was fitted to predict WLBMFA-based whole-brain *H* from DFA-based whole-brain *H*. A significant regression equation was found with an intercept of 0.018 and a coefficient of 1.073, $F(1, 93) = 98.25$, $p < .001$, $R^2 = .514$. Our results replicated findings in previous studies applying both DFA and wavelet approaches (Churchill et al., 2014) and demonstrated that 1) *H* calculated from DFA and wavelet approaches are closely related; 2) wavelet approaches exhibit a higher degree of variability, and in our sample, produced a greater number of extremely high *H* values; and 3) the regression equation for predicting wavelet-based *H* from DFA-based *H* often yields coefficients greater than 1.

Figure 5

Linear regression between DFA-based and WLBMFA-based whole-brain H

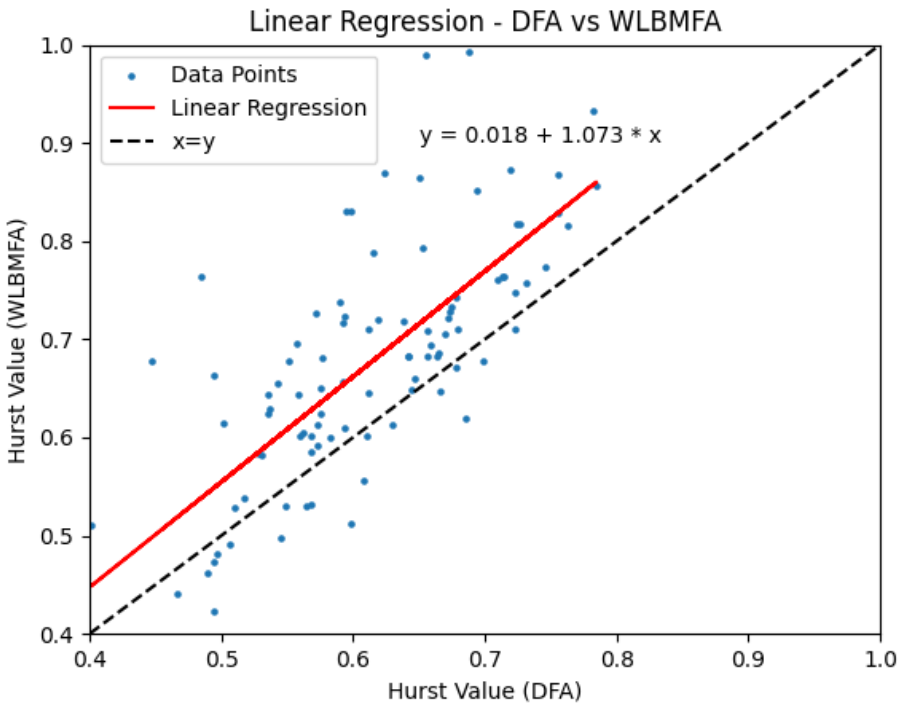

Note. The results revealed a significant regression equation with an intercept of 0.018 and a coefficient of 1.073 ($F(1, 93) = 98.25$, $p < .001$, $R^2 = .514$), indicating that whole-brain *H* from WLBMFA can be reliably estimated using DFA-based measures.

In accordance with the high correlation, the WLBMFA approach yielded comparable results in mixed effect models. Specifically, there were no main effects observed for either sedation level ($F(3, 91) = 0.84$, $p = .478$) or narrative listening ($F(1, 94) = 1.91$, $p = .171$; see *Figure 6*). A similar interaction effect was identified ($F(3, 79) = 3.66$, $p = .016$), suggesting a potential quadratic ($t(78) = 2.09$, $p = .040$) or cubic ($t(80) = -2.09$, $p = .040$) relationship between sedation level and whole-brain *H* only in the narrative listening condition (see *Figure 7*).

These results provided evidence that the mono-fractal relationship assumed in the DFA analysis was sufficient to capture participants' brain activity. This finding, along with the advantages of DFA described in *Methods*, supported our decision to move on with DFA results.

Figure 6

Whole-brain Hurst main effects of sedation level and narrative listening – wavelet

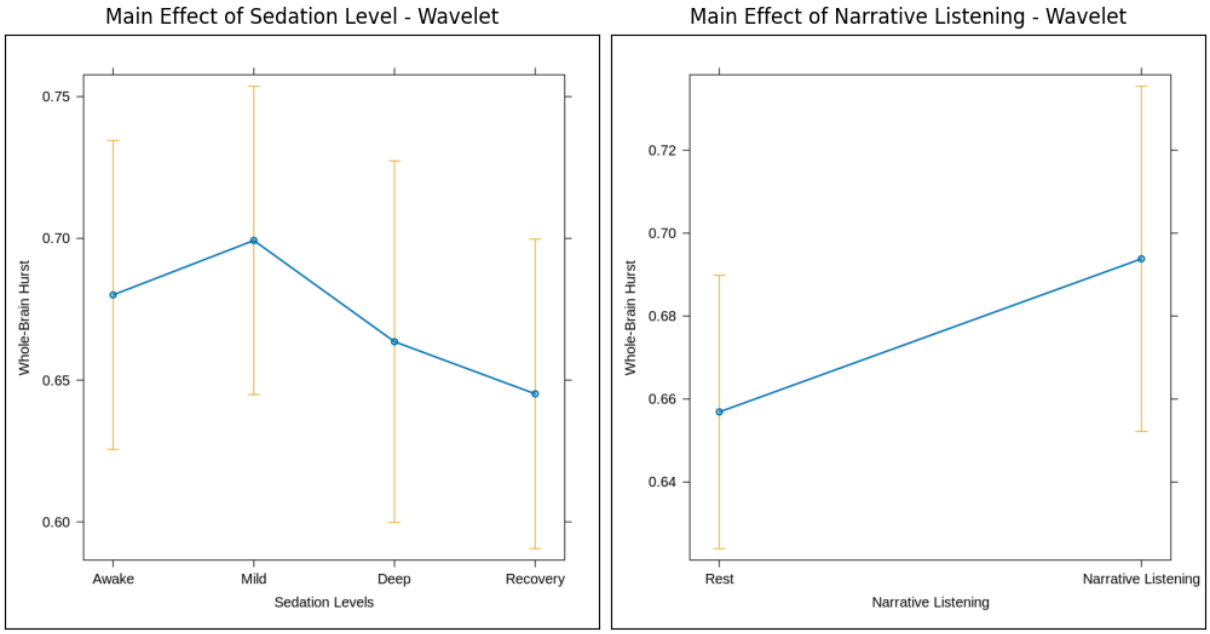

Note. Left: there was no significant main effect for sedation level ($F(3, 91) = 0.84$, $p = .478$). Right: there was no significant main effect for narrative listening ($F(1, 94) = 1.91$, $p = .171$).

Figure 7

Whole-brain Hurst interaction effects – wavelet

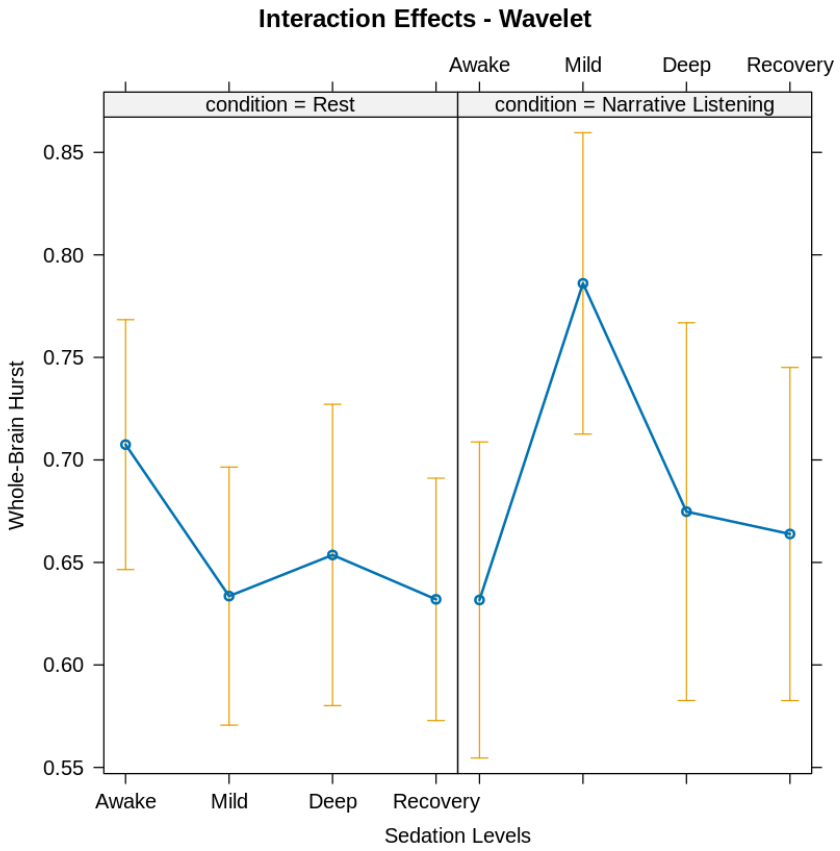

Note. The results obtained from the wavelet approach were consistent with those generated from DFA. A slight deviation in the pattern was observed in the recovery level. It is possible that during the recovery phase, the brain activity of participants is less amenable to a mono-fractal analysis. Nevertheless, the difference was not statistically significant.

The Latent Variable of Propofol

We used PLS to find the latent variable representing the effect of propofol. However, in the rest condition, we failed to find any significant latent variable (p = 0.139, crossblock covariance = 54.698%; see *Supplementary Figure 2*). It is possible that the effect of propofol during the resting state, as measured by H, is too subtle to be discerned, or may necessitate a larger sample size to detect.

In contrast, in the narrative listening condition, PLS analysis identified a single statistically significant latent variable representing the effect of propofol ($p < 0.001$, crossblock covariance = 79.316%; see *Figure 8*). To assess the stability of the results, we set the threshold for stability as absolute bootstrap ratios > 3 (which is akin to a Z-score confidence interval of 95%), and only brain areas with a statistically stable loading were considered significant and selected for brain plotting. All stable nodes displayed a positive loading. The right panel in *Figure 8* displays the actual *H* values for these stable brain nodes. The observed correlation between the latent variable and sedation level, as well as the actual *H* values for the significant brain nodes, showed a consistent pattern: *H* increased from awake to mild, peaked at mild sedation, and then gradually returned to the baseline (awake). In addition, we used all scanning sessions in a single PLS model (i.e., including 2 conditions and 4 sedation levels), and the results were consistent with our previous findings from the separate analyses (see *Supplementary Figure 3*).

Figure 8

Latent variable of propofol during narrative listening

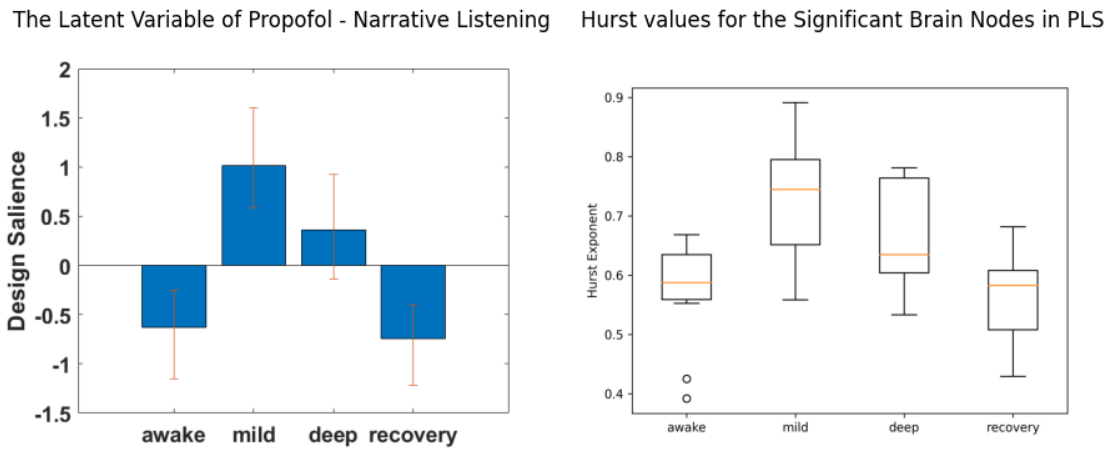

Note. The left panel displays a single significant latent variable explaining approximately 79% of the crossblock covariance. An inverted U-shaped Hurst-Propofol gradient can be detected where the *H* value reached its peak during mild sedation. The bar plot presented in the right panel illustrates the average *H* values for the stable brain nodes (bootstrap ratio > 3) in the PLS model for narrative listening, which aligns with the trend observed on the left.

In our analyses of the spatial pattern of the significant brain nodes, we found that the major nodes with the highest brain loadings were clustered within the bilateral occipitoparietal cortices, including the primary and secondary visual cortex, and extended to motor areas in the parietal cortex, such as the premotor cortex and primary motor cortex. The most affected areas further projected to parts of the bilateral posterior cingulate cortex, left frontal cortex, and subcortical structures, such as the corpus callosum and thalamus. All the stable brain loadings were positive, meaning that these brain nodes operated in the same direction of the inverted U-shape we observed in the whole-brain *H* section.

Figure 9

Brain plotting of stable brain nodes in PLS

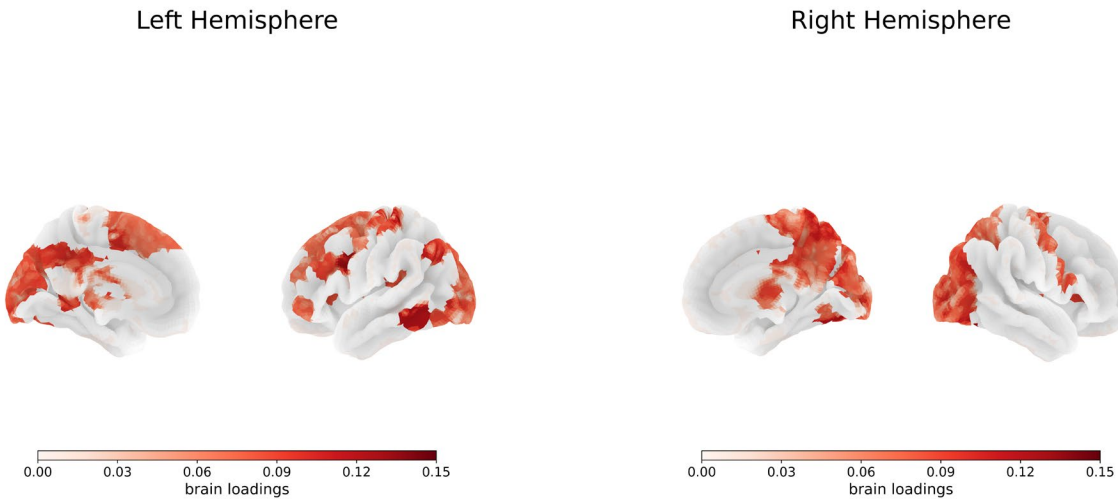

Note. This figure portrays the spatial distribution of the significant brain nodes superimposed on a brain template. The left panel corresponds to the left hemisphere, and the right panel corresponds to the right hemisphere. Brain plotting unveiled the bilateral occipitoparietal area and right premotor cortex as the brain regions with the highest brain loadings. This pattern of brain activity is reminiscent of the well-documented dorsal attention pathway, which is frequently implicated in visuospatial processing and attentional control.

Intuitively, the spatial pattern matches the well-documented dorsal visual attention pathway. To quantitively evaluate the pattern, we employed two approaches. First, we examined similarities between the latent variable of propofol and probabilistic meta-analysis maps from Neurosynth. Neurosynth aggregates data from over 14,000 published neuroimaging studies and enables the generation of brain maps that represent the regions most consistently associated with

specific psychological concepts or tasks, making it a reliable tool for neural-based classification. We used a previously defined subset of 123 terms (e.g., “attention”, “response inhibition”, “navigation”) which was restricted to the overlap between Neurosynth terms and Cognitive Atlas terms (Hansen et al., 2020; Stier et al., 2021). Each term’s association map was correlated with the latent variable of propofol, and significance was assessed via a spatial null model (see *Methods*). Only two terms survived family-wise error rate correction and one of them, unsurprisingly, was visual attention (see *Figure 10*).

Visual attention was found to be positively correlated with the propofol gradient whereas stress was found to have a negative correlation with the propofol gradient. The original association maps of the two significant terms can be found in *Supplementary Figure 4*. Second, we applied the 8-network mask to filter the significant brain nodes. This mask was developed by Shen et al. (2013) along with the 268-parcellation and includes the default mode network, frontoparietal network, medial frontal network, motor network, subcortical-cerebellar network, visual association network, and primary and secondary visual network. While neither the one-way analysis of variance (ANOVA; $F(7, 51) = 1.58$, $p = .162$) nor hypergeometric tests ($p = .373$ - .749) showed a significant difference across networks, the networks that involve visual attention and motor movement, such as the frontoparietal, secondary visual, and motor network, still ranked among the top affected networks, which is consistent with the Neurosynth analysis (see *Figure 9*).

Figure 10

Significance of Neurosynth terms via spatial null model

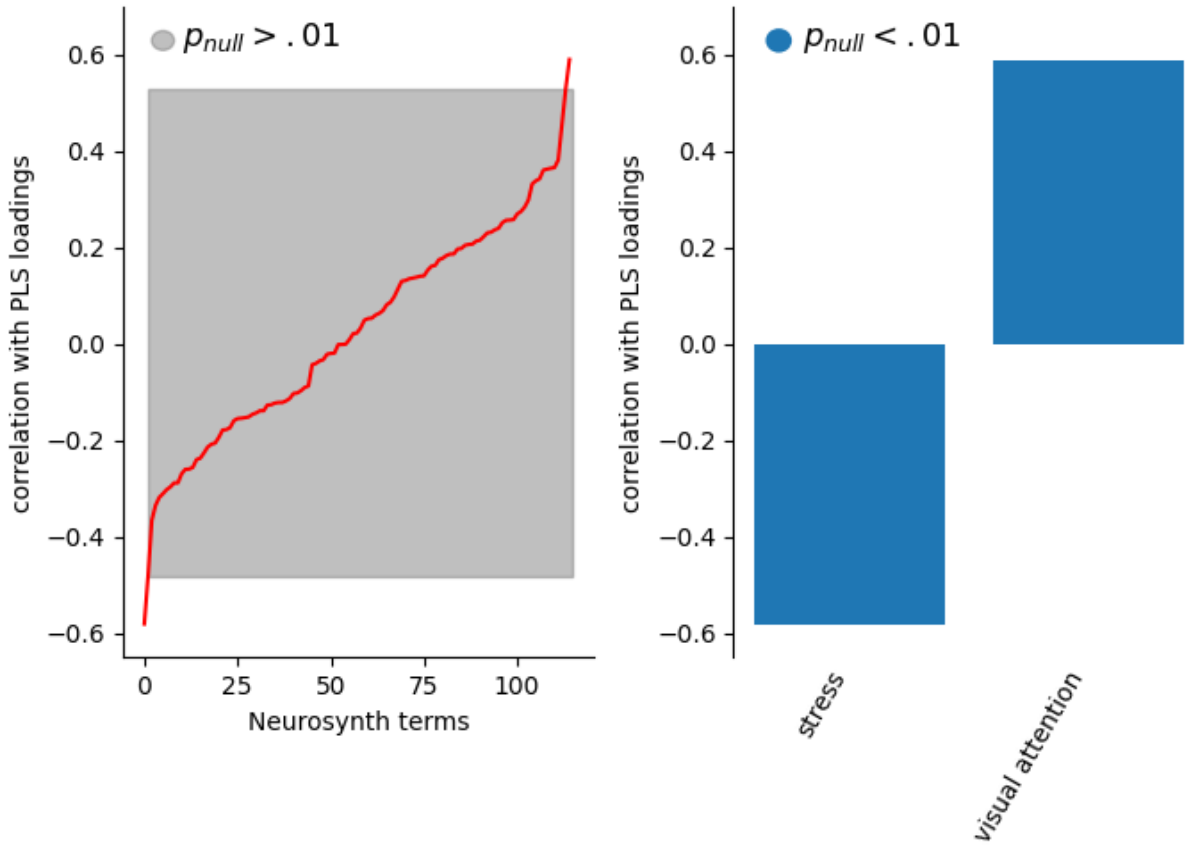

Note. The left panel illustrates the results of 10,000 parametric spatial permutation tests, with non-significant terms shown in grey (Benjamini-Hochberg correction, $\alpha = 0.01$). The terms are ranked by the magnitude of their correlations. In contrast, the right panel highlights the two significant Neurosynth terms: visual attention displayed a positive correlation with the latent variable of propofol, while stress exhibited a negative correlation. It is important to note that these Neurosynth maps only show which regions are commonly reported alongside a given term, and do not indicate the sign of the association (i.e., whether the psychological term is associated with functional activation or deactivation).

Figure 11

Network masking for narrative listening

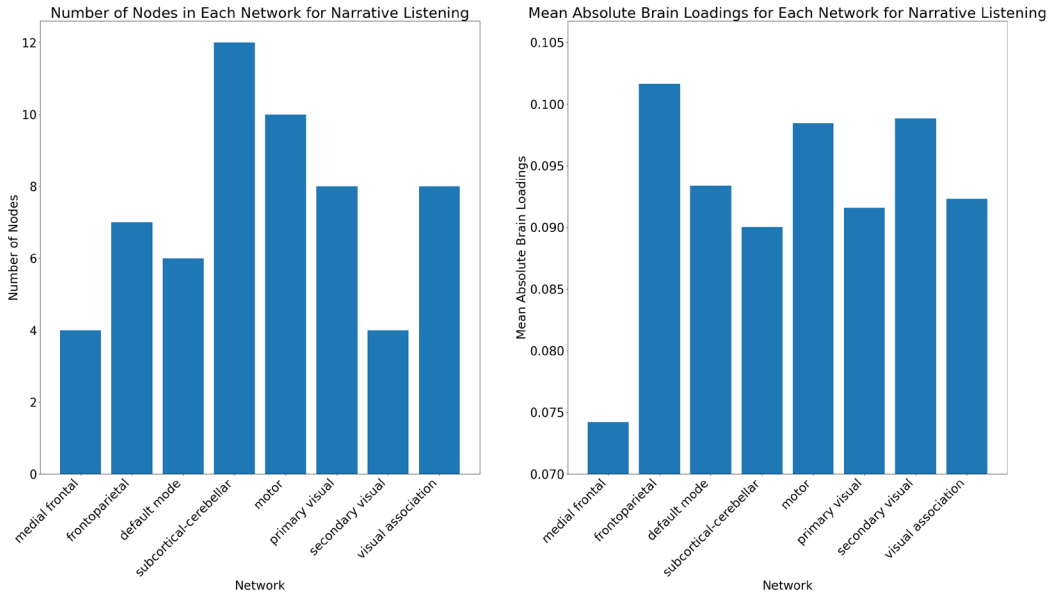

Note. Interestingly, the number of significant nodes and the mean absolute brain loadings in each network yielded different rankings, which implied that the most extensively involved networks may not be the most rigorously involved ones. While ANOVA did not reach statistical significance, this finding may still provide valuable information regarding to the most relevant brain networks involved in sedation.

The Moving Window Approach

The moving window approach is particularly productive in anesthetic research because of the nuanced temporal gradients for different drugs to take effect (Eagleman et al., 2019; Won et al., 2019). This approach is most frequently applied in the analysis of physiological data (e.g., EEG, heart rate) to obtain a smoother trend over time (Eagleman et al., 2019; Maksimow et al., 2014; Tarvainen et al., 2012; Won et al., 2019). There are fewer studies taking moving windows

in neuroimaging data (Amico et al., 2014; Luppi et al., 2019) and none of them applied Hurst analysis. It is worth noting that DFA has been found to highly reliable in dealing with shorter signals, which is well-suited for moving window analysis of neuroimaging data (Oświęcimka et al., 2006). Therefore, applying DFA to moving windows appears to be in a vacuum with brimming potential.

In the present study, we applied Hurst analysis to every 60 TR as a moving window in each scanning session to obtain *H* values across time. That is, each window was defined as a consecutive sequence of 60 TRs, with the first window ranging from the 1st to the 60th TR, the second window ranging from the 2nd to the 61st TR, and so on. As the narrative listening condition contained only about 150 volumes, we selected the first 90 windows across all scanning sessions, representing the 1st to 150th TR, to ensure data comparability and avoid missing data. Next, we performed *t*-tests between the whole-brain *H* of each individual window with that of the first window to obtain whole-brain *H* fluctuations across time using the first window as an anchor point. This revealed statistically significant deviations in *H* over the course of each scan. The *H* value fluctuations are shown in *Figure 12*.

Overall, whole-brain *H* values rose immediately after the start of the scanning session, regardless of the participant's sedation level or exposure to the narrative. This finding supported our hypothesis that external stimuli, such as verbal communication, still had an impact on participants early in the scanning session. To quantify the magnitude of *H* fluctuations, we plotted the *t*- and *p*-values in iterative *t*-tests against window number in *Figure 13*. Notably, participants in the narrative listening condition appeared to be more susceptible to the effects of propofol. In the resting condition during deep sedation, the *p*-value never fell below the significance threshold, indicating that the waning of external stimuli did not significantly

influence participants. Conversely, for the narrative listening condition, the *p*-value for awake, mild, and deep sedation displayed a clear pattern where it dropped below the significance threshold in roughly 20 TRs (40 seconds) and remained below this threshold in a relatively stable manner. Interestingly, the first time at which these *p*-values dropped below the significance threshold increased monotonically, from 9th window while awake, 10th window during mild sedation, 21st window during deep sedation, to 50th window during recovery.

Figure 12

Temporal dynamics of H values across all scanning sessions

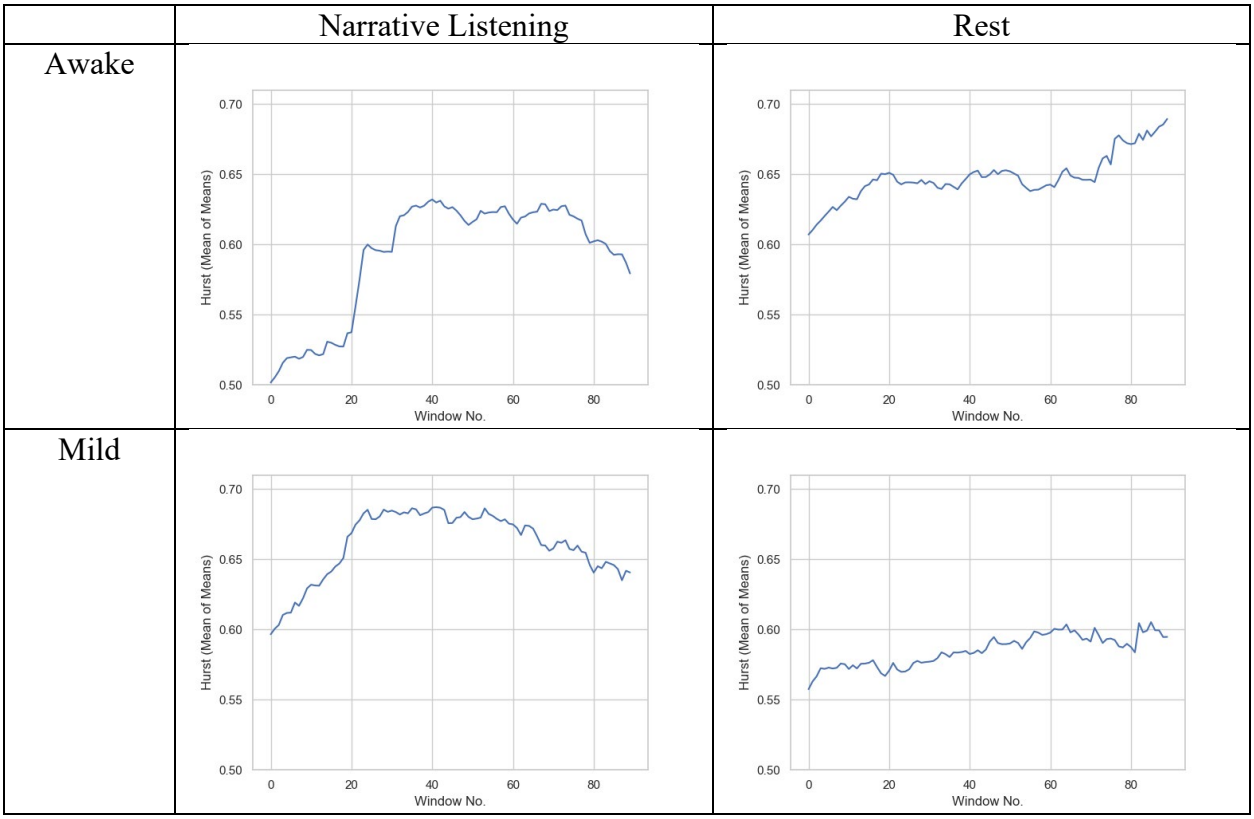

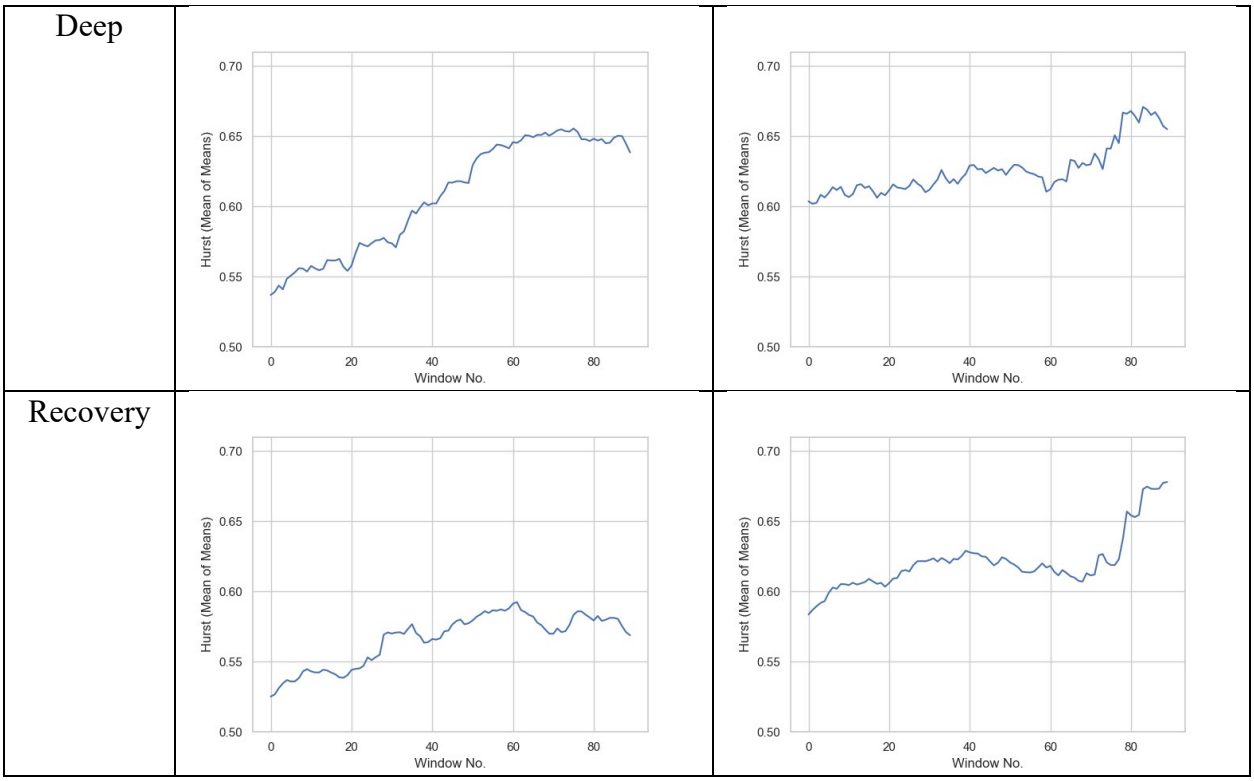

Figure 13

Temporal dynamics of t- and p-values in iterative t-tests across all scanning sessions

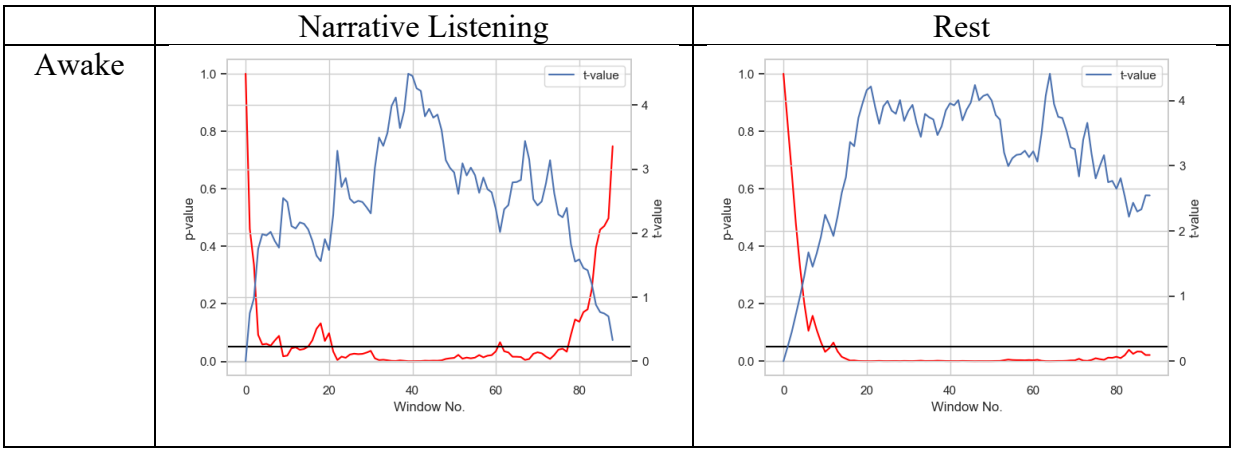

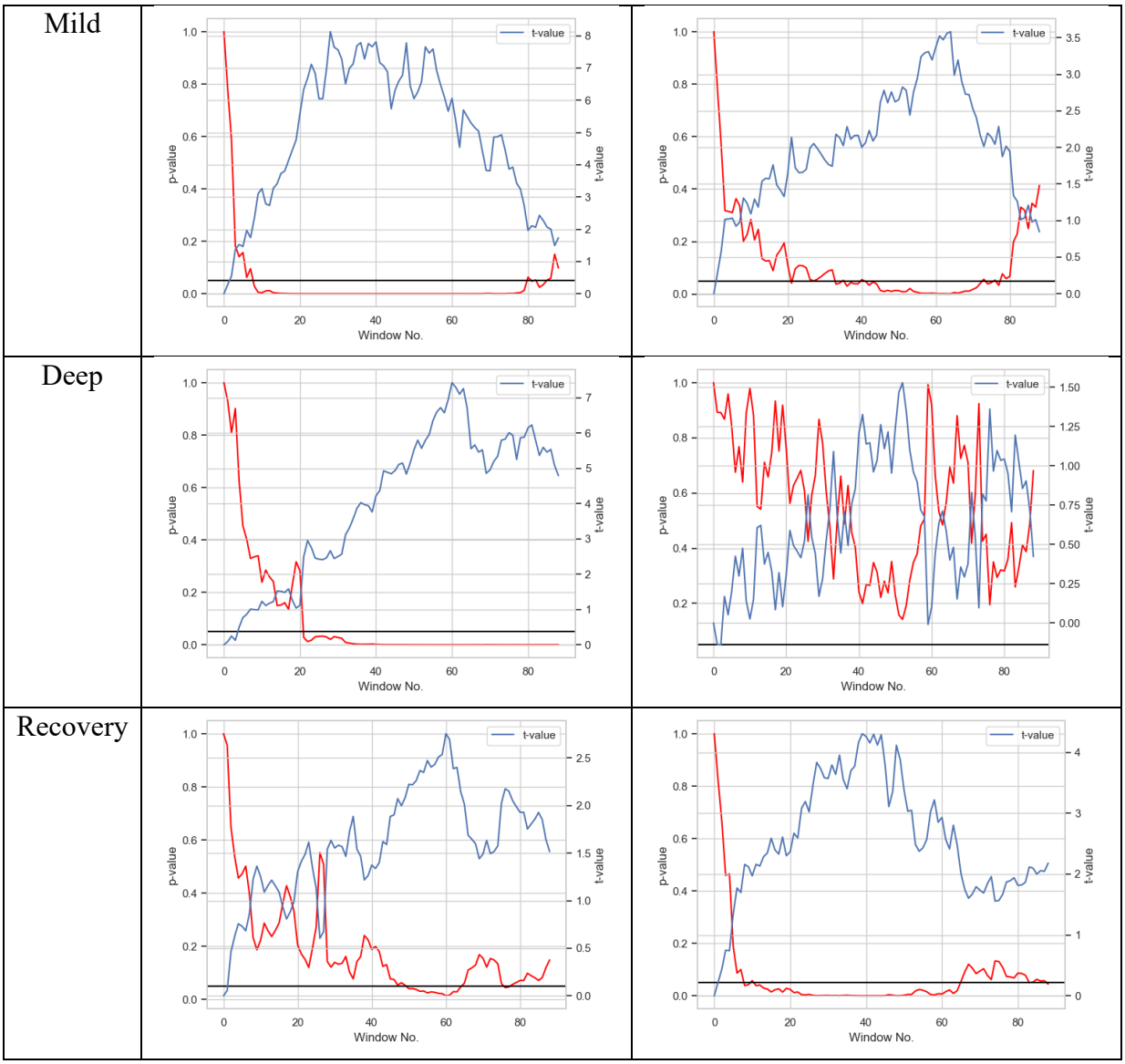

Note. The blue line represents t-values while the red line represents *p*-values. The black horizontal line is $p = .05$.

Another line of evidence supporting the significant distinction between brain activities early and late in the same scanning session was obtained from the spatial correlation of brain loadings. For this analysis, we selected the mild and deep sedation sessions in the narrative listening condition because 1) the latent variable of propofol was only significant in the narrative listening condition; 2) the *p*-value was most stable under the significance threshold after 20 TRs

for these two sessions; 3) they had a lower risk of introducing confounds due to the unknown, noisy effects of recovery. We selected every 10 windows in *Figure 12* and *13* as the window of windows, so that the first new window consisted of the 1st to 10th window in the previous procedure. We then conducted iterative PLS analyses on the 268 brain nodes in 81 newly created windows, in order to identify a latent variable between each new window and the first new window. The temporal trend of the PLS model's *p*-value is presented in *Figure 14*, which perfectly corresponds to the pattern in *Figure 13*. After 10 TRs for the mild sedation session and 20 TRs for the deep sedation session, the PLS model achieved statistical significance and remained below the threshold throughout the rest of the session. We then extracted the brain loadings of each PLS model and estimated their correlations with the brain loadings in the first PLS model (i.e., 1st new window against 2nd new window). The significance of each correlation was again assessed using a spatial null model with 10,000 permutations. The results are summarized in *Figure 15*. Although there seemed to be a delay in the change of spatial activation patterns, these results nevertheless indicated that after approximately 50 new windows (around 110 TRs, or 3.5 min), the spatial pattern of brain activation was no longer significantly associated with the pattern in the beginning of the scanning session. In conclusion, the results from brain-wise *t*-tests, PLS significance across time, and the fluctuations in brain loadings all provide evidence that brain activity in the beginning of a scanning session is qualitatively different from that later into the scanning session. At the extreme, it is even possible to say that the brain activity at two time points during a single scanning session may be unrelated.

Figure 14

Temporal dynamics of p-values in iterative PLS

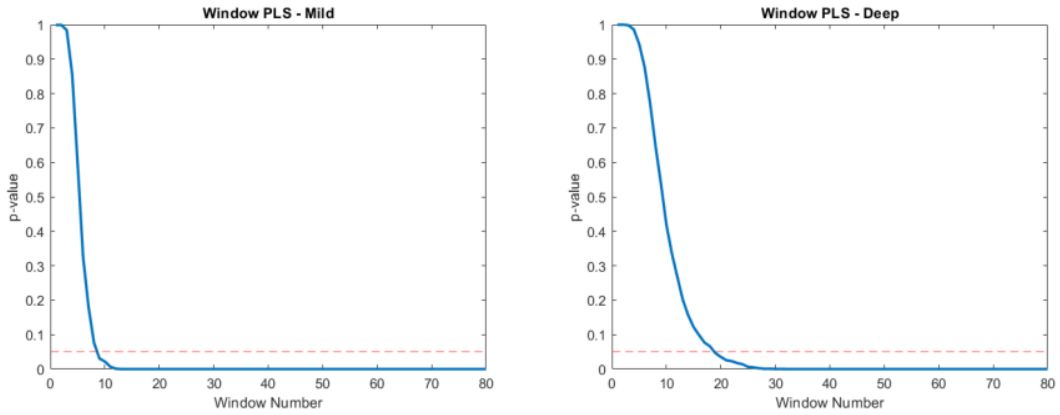

Note. The *p*-values for the PLS model sharply declined from the onset of the scanning session. Specifically, after 10 TRs for the mild sedation session and 20 TRs for the deep sedation session, the PLS model achieved statistical significance and remained below the threshold throughout the rest of the session.

Figure 15

Temporal dynamics of spatial correlations of brain activation patterns

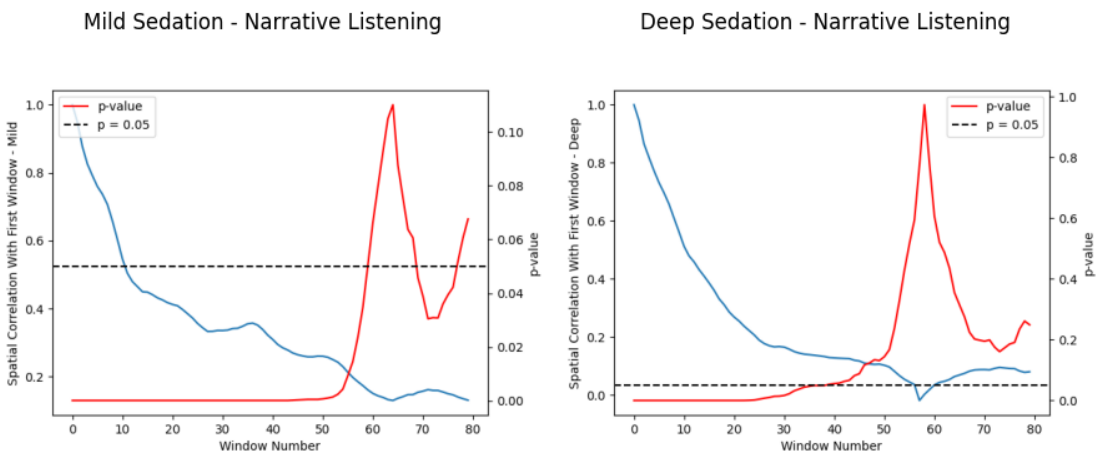

Note. The brain loadings of the first PLS model were correlated with those of each individual model using Spearman's rank correlation. The *p*-value was assessed using the spatial null model with 10,000 permutations. Although not identical to the previous two figures, this figure demonstrated that the spatial pattern of activation underwent significant changes after approximately the 50th window.

Having confirmed the existence of temporal dynamics of *H* within a single scanning session, we proceeded to perform a PLS analysis on specific aggregated windows at the beginning ("early": 1^{st} – 6^{th} window for mild sedation and 1^{st} – 20^{th} window for deep sedation in *Figure 13*) and in the middle ("late": 41^{st} – 46^{th} window for mild sedation and 41^{st} – 60^{th} window for deep sedation in *Figure 13*) of the scanning session. As depicted in *Figure 16*, both PLS models revealed a single latent variable representing the time course of the scanning session ($p < 0.001$, cross-block covariance = 100% for both). While the areas around the bilateral occipitoparietal cortex remained significantly related to the latent variable, temporal areas, which

were absent from the whole narrative listening model, were somewhat involved (see also *Supplementary Figure 5*). No Neurosynth terms survived family-wise error rate correction.

One-tailed hypergeometric tests were used to test for significant differences in the count of significant nodes in each network. Benjamini/Hochberg correction was employed to account for multiple comparisons. The results revealed that in the mild sedation session, the subcortical-cerebellar network showed a statistically significant greater count of significant brain nodes ($p < .001$), followed by the motor network ($p = .040$), compared to other networks. In the deep sedation session, the subcortical-cerebellar network also had more significant brain nodes than other networks ($p = 0.007$, see *Figure 17*).

One-way ANOVA detected a significant inter-network brain loading difference in the early versus late model in only mild ($F(7, 99) = 3.492$, $p = .002$) but not deep ($F(7, 63) = 1.74$, $p = .115$) sedation session of the narrative listening condition. Post-hoc Tukey's Honestly Significant Difference (HSD) tests, which automatically adjust for multiple comparisons, revealed that the mean absolute brain loading of the frontoparietal network was significantly higher than that of the subcortical-cerebellar ($p = .048$) and the default mode network ($p = .012$) during mild sedation. The medial frontal network also had higher loadings than the default mode network ($p = .030$). All the windows were taken from the narrative listening condition.

Our intriguing findings suggest that the subcortical-cerebellar network was broadly but only superficially modulated by propofol within a relatively short time window (within 2 min). This modulation may have occurred as a peripheral effect of altered activities in other brain regions. In contrast, the frontal areas, including the frontoparietal and medial frontal network, had a higher average brain loading for each significant brain node at least during mild sedation. This differential effect of propofol on the frontal and subcortical-cerebellar networks may be a

result of the highly specialized functional localization and targeted modulation by propofol in the frontal areas. These results further emphasize the modulation of higher-order cognitive functions by propofol, as the targeted frontal networks are commonly associated with attention, working memory, and cognitive control (Marek & Dosenbach, 2022; Markett et al., 2013).

Figure 16

Early versus late window PLS and brain plotting

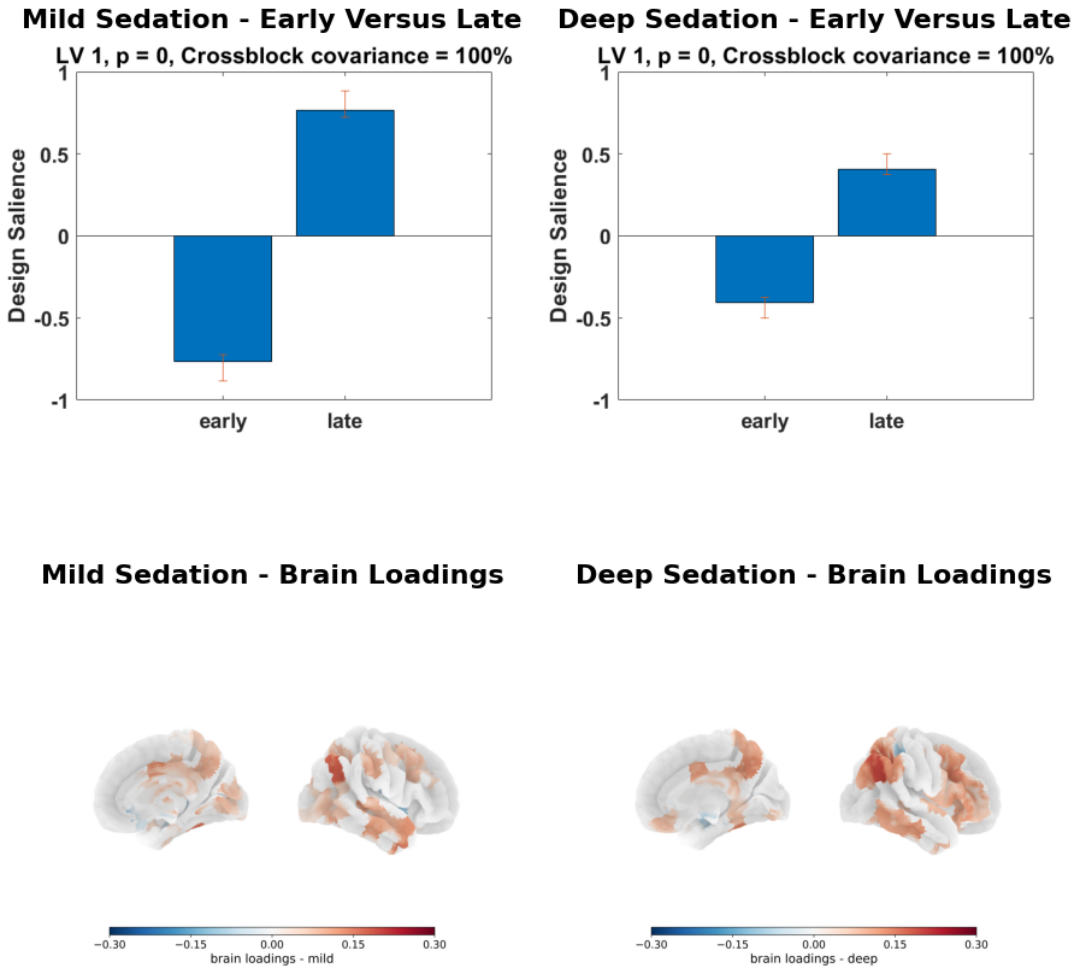

Note. The upper section of this figure presents the PLS results for the comparison between early and late stages in both mild and deep sedation sessions during the narrative listening condition. The results were significant, with a single latent variable representing the time course. The lower section displays the significant brain nodes with stable brain loadings. Interestingly, the most affected brain areas also appear to be centered in the occipitoparietal cortex, but with additional temporal nodes identified in the early vs. late models.

Figure 17

Network masking for early versus late models

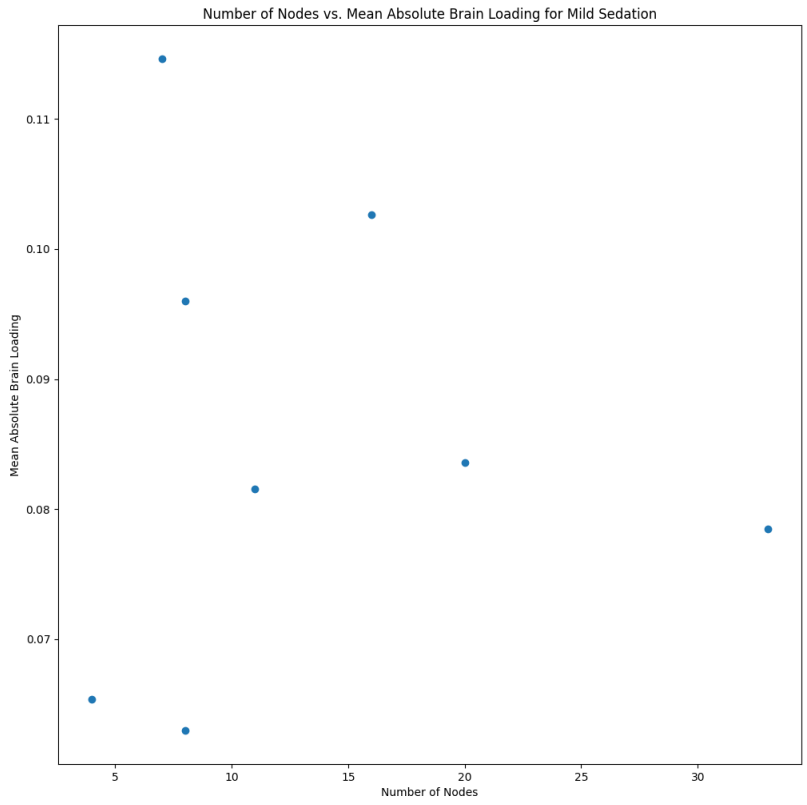

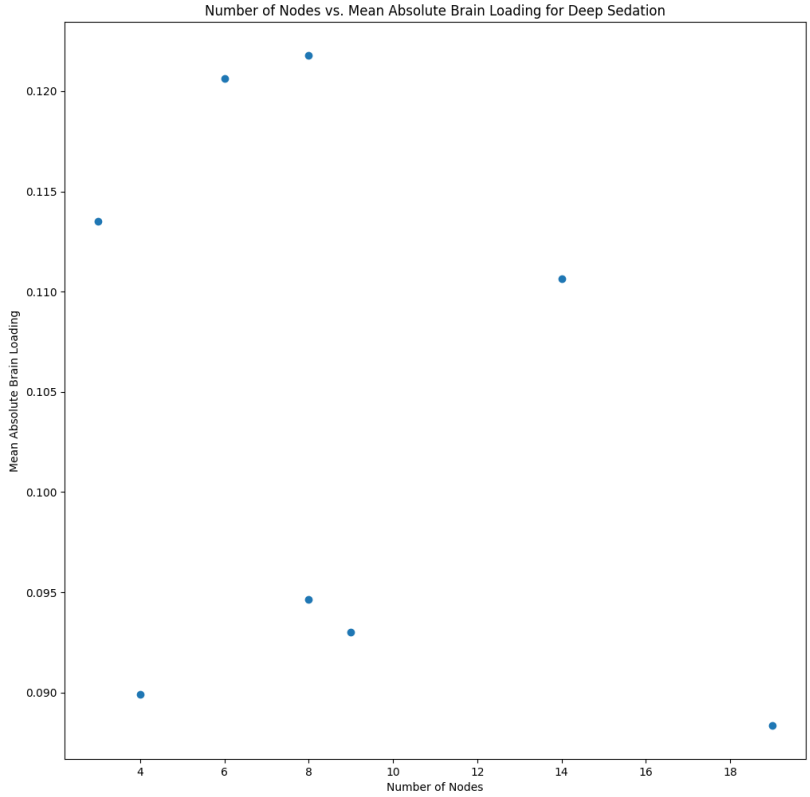
Number of Nodes vs. Mean Absolute Brain Loading for Deep Sedation
Mean Absolute Brain Loading
0.120
0.115
0.110
0.105
0.100
0.095
0.090
4
6
8
10
12
14
16
18
Number of Nodes

Mild Sedation - Brain Network

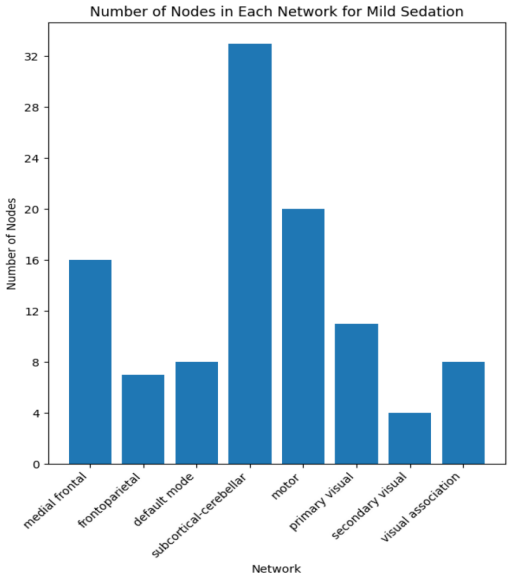

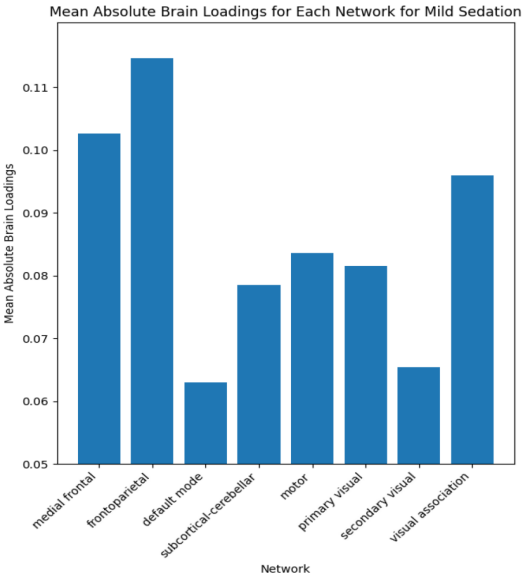

Deep Sedation - Brain Network

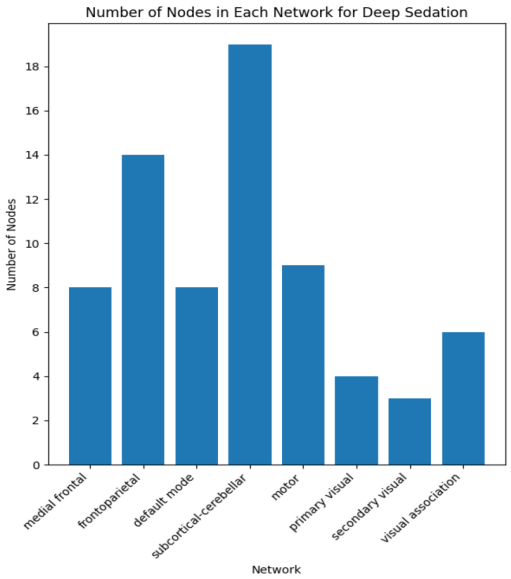

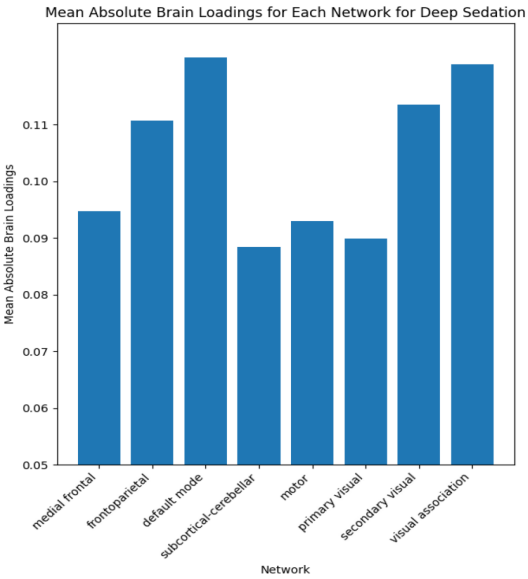

Note. This figure provides an overview of the number of nodes and the average absolute brain loadings for both the mild and deep sedation sessions in each of the eight networks. The subcortical-cerebellar network was found to have the highest number of significant brain nodes, while the frontoparietal network had significantly higher mean brain loadings in the mild sedation session compared to the other networks. Notably, although not reflected in statistics, we saw a surge in the mean brain loadings in the default mode network from mild to deep sedation.

Discussion

We discuss our findings from the four following aspects of our results: 1) the inverted U-shape of whole-brain *H*; 2) the differential effect of propofol on *H* between resting state and narrative listening; 3) the lack of involvement of auditory cortices; 4) the involvement of visual attention in absence of visual stimuli and the mental imagery hypothesis.

Inverted U-Shape of Whole-Brain *H*

It was unexpected that a main effect of narrative listening was no observed, contrary to the well-documented literature on task/rest, sleep/wakefulness, and stress, where a more relaxed state is typically associated with higher *H* values (Acharya et al., 2005; Churchill et al., 2016; He, 2011; Wei et al., 2013). Theoretical framework of criticality also supports this directionality, as cognitive resource allocation is expected to be less stringent during rest, when the brain is in closer proximity to the critical state. Although DFA results were consistent with these predictions, the wavelet approach generated a reversed pattern. Since both comparisons were nonsignificant, we should avoid overinterpreting null results and treat them as random noise. One possible explanation concerns the interleaved design in which there was no break between scanning sessions. Previous research utilizing Hurst analysis has shown that brain dynamics

measured by *H* may take up to 15 minutes to normalize, depending on the cognitive load of the task (Barnes et al., 2009). It is plausible that the baseline *H* for the resting state condition was somewhat contaminated by residual effects of narrative listening, and rather than reflecting a true resting state, *H* values during resting state may represent a normalization process from any carry-over effects.

In the narrative listening condition, our findings indicated that *H* followed an inverted U-shaped curve where *H* was higher during sedation than wakefulness but peaked during mild sedation rather than deep sedation. If we interpret deep sedation as a state resembling later stages of sleep, our findings are in line with previous studies investigating *H* during sleep, which have shown that later sleep stages could be characterized by lower *H* (Acharya et al., 2005; Song et al., 2007). Multiple lines of evidence in our results point to propofol's modulation of executive functions (e.g., attention, cognitive control) as a possible explanation – 1) the spatial pattern of significant brain nodes in the narrative listening condition represented a visual attention pathway as validated using Neurosynth terms; 2) components of the dorsal visual attention pathway are qualitatively involved in the inter-session model in a funnel-like top-down manner, with the frontoparietal and subcortical-cerebellar network appearing to be the most rigorously and the most extensively affected network, respectively; and 3) when taking a closer look at the nuanced temporal gradient within each scanning session, the same pattern for the subcortical-cerebellar and frontoparietal network became quantitatively justified. According to Shen et al. (2013)'s 8-network mask, the frontoparietal network is comprised of the dorsolateral prefrontal cortex (DLPFC), the posterior parietal cortex (PPC), and adjacent areas, all of which have been consistently associated with cognitive control (Motzkin et al., 2014; Vincent et al., 2008; Wang et al., 2010). The cerebellar-subcortical-cortical system has also been implicated in the

modulation of a variety of complex cognitive functions, including executive control, adaptive learning, and attention (Clark et al., 2021; Brissenden & Somers, 2019). An elevated cognitive activity, as indicated by the reduction of *H* during deep sedation, might be attributed to loosened frontal control over the brain and the consequent emergence of anticorrelated, unsupervised, and/or spontaneous processes. These findings provide evidence against the linear progression model of sedation. Anesthetic agents may have a graded effect on specific brain areas or cognitive tasks, but globally, our findings do not support the simplistic assumption of linear deactivation across time (Adapa et al., 2014).

Differential Effect of Propofol on *H* Between Resting State and Narrative Listening

Regardless of data quality concerns, another takeaway from this study is that participants appeared to be less affected by propofol during resting state compared to narrative listening. Our PLS analysis did not yield significant results for the resting state condition and, importantly, the within-session time courses in *Figure 13* also showed less variation for the resting state, especially during mild and deep sedation. The latter observation could not be simply explained by data contamination because we would expect to see more, rather than less, variation if the waning of residual effects from narrative listening presented in addition to the standard normalization process. The differential effect of propofol between resting state and narrative listening may be explained by revisiting the concept of *H* as an index for the proximity to the critical state. Propofol, as a sedative, acts to modulate brain activity towards a state of rest and induce a return to the critical state. During narrative listening, participants direct their attention to the movie excerpt and dedicate cognitive resources in relevant brain areas for thorough comprehension of the script. This can lead to a drift away from the critical state, which is characterized by massive flexibility. Conversely, during the resting state, the cognitive control

system does not experience a high demand for directing attention and processing incoming information, and thus the brain should be inherently closer to the critical state. We believe that the baseline difference in the proximity to the critical state, although not reflected as a significant main effect, nonetheless explains the lower observed variance during the resting state.

Lack of Involvement in Auditory Cortices

Surprisingly, we found limited evidence for the involvement of auditory cortices, which is frequently reported in the literature (Dueck et al., 2005; Plourde et al., 2006). The primary and secondary auditory cortex, as well as the auditory association cortex, showed minimal association with the temporal gradient of *H* during sedated narrative listening, nor did Wernicke's area exhibit any relevance. Although the within-session analysis revealed some involvement of temporal areas, their absolute brain loadings were relatively low. Therefore, our results demonstrate that the effects of propofol on auditory cortices were at best small and transient, if not non-existent, as measured by the *H*.

One possible way to explain this divergence between previous research and the current findings concerns the statistical properties of *H*. Hurst analysis provides exquisite temporal resolution at the cost of losing spatial details. In both DFA and WLBMFA, each brain node is treated as a single, independent unit for analysis. Although we used the spatial null model to compensate for the loss, *H* still retains very little information about the inter-region connectivity. However, many studies have attributed the loss of consciousness during sedation to the breakdown of effective cortical connectivity instead of the functional deactivation in specific areas (Chamberlain & Rosenberg, 2022; Ferrarelli et al., 2010; Hudetz & Imas, 2007; White & Alkire, 2003). For example, Liu et al. (2012) demonstrated that the inferior frontal gyrus remained functionally connected to a wide range of frontoparietal and temporal neural

organizations regardless of propofol administration, suggesting a retained high-order processing network for verbal comprehension and memory. The change lay in the disconnection of frontal areas from the primary auditory cortex during deep sedation, leading to a lack of information integration rather than information collection. Thus, we recommend future research to explore ways for integrating temporal dynamics with spatial connectivity.

Involvement of Visual Attention in Absence of Visual Stimuli – Mental Imagery Hypothesis

Equally surprising was the pronounced engagement of the visual systems during sedated narrative listening, despite the absence of visual stimuli. In the PLS model, significant brain nodes were predominantly clustered around the occipitoparietal areas and motor areas. Spatial correlation with Neurosynth terms also revealed the visual attention pathway as a significant spatial pattern. In conjunction with subsequent network masking and within-session analyses, we saw a fairly complete picture of visual processing, with significant nodes from both lower-end structures (e.g., the primary and secondary visual cortex) and integrative organisms (e.g., DLPFC, the visual association cortex, precuneus).

One question that remains is why participants exhibited visual activation without actual visual stimuli. We propose the mental imagery hypothesis as a potential explanation. Mental imagery refers to the ability to visualize objects outside of one's line of sight (Kosslyn et al., 2001). Traditionally, mental imagery has been conceptualized as a process that requires voluntary control to sustain selective attention and execute complex cognitive tasks such as language comprehension (Monti et al., 2010). Most classic mental imagery studies also require the participant to be conscious and behaviorally responsive regardless of the task (Ganis et al., 2004; Kosslyn et al., 1999). Can mental imagery be generated unconsciously? In a review by Pearson et al. (2015), that question was left open. More recently, researchers have begun to

report some success in dissociating behavioral responsiveness and mental imagery abilities. Particularly relevant to our discussion is the study by Huang et al. (2018), in which they found fMRI signatures of mental imagery in one participant who received propofol administration and were behaviorally unresponsive. In that study, participants were asked to perform three mental imagery tasks: tennis, navigation, and hand squeeze, along with a motor response task – real hand squeeze. The task instructions were also presented verbally using a computer software. One out of five participants in that study displayed robust fMRI signatures of mental imagery in tennis and hand squeeze after loss of responsiveness. Although this study had limitations in terms of their sample size and percentage of significant results (only 1/5), they nevertheless provided preliminary evidence for the disassociation between mental imagery and consciousness, which echoes with our results. The inverted-U shape pattern found in the current study may even suggest that the mental imagery process is more active during deep sedation than mild sedation, potentially because of loosened cognitive control in frontal areas.

Moving to visual mental imagery (VMI) in particular, the prevailing models propose that the early visual cortices (V1-V3) are most responsible for generating VMI (Kosslyn et al., 2001; Pearson et al., 2015). According to this model, the basic elements of VMI, such as spatial and sensory representations, are naturally synthesized at lower levels of the brain, making early processing networks essential for the generation of VMI. However, a series of double dissociation lesion studies have challenged this claim (Bartolomeo, 2008; Moro et al., 2008). Subsequent studies and reviews have continued to find that, compared to early visual processing areas, higher-order structures, particularly the frontoparietal cortex, are more crucial for VMI (Bartolomeo et al., 2020; Liu et al., 2021). A meta-analysis of 46 fMRI studies on VMI concluded that only the frontoparietal network and a well-delimited region in the left fusiform

gyrus are consistently involved in VMI (Spagna et al., 2021). We do not intend to solve the debate here as it is outside of the scope of this study, but it seems plausible to us that both "early" and "late" structures in the visual processing system can be somewhat involved during VMI. No matter which model we adopt, the fact that we are seeing a complete visual processing pathway from primary visual areas to frontal areas suggests that the modulation of VMI abilities by propofol at least partially accounts for the fluctuation of *H* observed across different sedation levels during narrative listening. From this perspective, the lack of sensory sources for mental imagery could also possibly explain the null results in the resting state condition. Even within a shorter time range as in moving window analyses, the frontoparietal network still seemed to be the target of propofol modulation. As environmental stimuli gradually waned, propofol tended to put this important "late" VMI structure into rest.

Limitations

While the findings of this study contribute to the understanding of the neural correlates of sedation, several limitations must be acknowledged. First, our sample size of 17 participants is relatively small, with each of the eight scanning session having only about 12-15 participants after controlling for motion and R^2. A larger sample size would be beneficial for future research. Second, as mentioned before, Hurst analysis does not account for the spatial connectivity between brain nodes. Hence, our results may not be accurate in reflecting inter-region information communications. Finally, the moving window approach may be susceptible to unquantifiable confounding variables embedded in the movie content. Although we found a relatively smooth trend within each session, we are unable to rule out the possibility that *H* fluctuations at certain time points might be caused externally by some particularly evocative episodes in the movie. In light of the limitations of this study, we recommend future

investigations with larger sample sizes to confirm the present findings and to enhance the generalizability of the results. Additionally, further studies could use experimental materials with different levels of emotional valence and arousal and utilize other neuroimaging analysis techniques that incorporate both temporal and spatial analyses to provide a more comprehensive understanding of the changes in brain dynamics induced by propofol.

Conclusion

In conclusion, our study investigated the temporal dynamics of Hurst exponent during propofol-induced sedation during narrative listening and resting state. Our findings suggest that brain activity during propofol-induced sedation does not follow a linear deactivation model, but rather a inverted U-shaped pattern during narrative listening. Surprisingly, we found little evidence for the involvement of auditory areas, while visual systems were highly engaged in absence of visual stimuli, which may be explained by visual mental imagery. Our use of the moving window approach allowed for a more fine-grained analysis of the temporal dynamics of brain activity. This approach also confirmed that the effects of pre-scanning stimulations can persist for up to 20 TRs. Furthermore, results from the moving window approach also highlighted the dynamic changes of specific brain networks, including the frontoparietal and subcortical-cerebellar networks, during a single scanning session. Overall, our study introduces Hurst analysis as a new statistical tool for analyzing neuroimaging data in the context of anesthetic research and provides a within-between session framework for future investigations of sedative agents.

References

Acharya U., R., Faust, O., Kannathal, N., Chua, T. L., & Laxminarayan, S. (2005). Non-linear analysis of EEG signals at various sleep stages. *Computer Methods and Programs in Biomedicine*, *80*(1), 37–45. https://doi.org/10.1016/j.cmpb.2005.06.011

Adapa, R. M., Davis, M. H., Stamatakis, E. A., Absalom, A. R., & Menon, D. K. (2014). Neural correlates of successful semantic processing during propofol sedation. *Human Brain Mapping*, *35*(7), 2935–2949. https://doi.org/10.1002/hbm.22375

Aggarwal, A., Brennan, C., Shortal, B., Contreras, D., Kelz, M. B., & Proekt, A. (2019). Coherence of visual-evoked gamma oscillations is disrupted by propofol but preserved under equipotent doses of isoflurane. *Frontiers in Systems Neuroscience*, *13*(19), 1–13. https://doi.org/10.3389/fnsys.2019.00019

Amico, E., Gomez, F., Di Perri, C., Vanhaudenhuyse, A., Lesenfants, D., Boveroux, P., Bonhomme, V., Brichant, J.-F., Marinazzo, D., & Laureys, S. (2014). Posterior cingulate cortex-related co-activation patterns: A resting state fmri study in propofol-induced loss of consciousness. *PLoS ONE*, *9*(6). https://doi.org/10.1371/journal.pone.0100012

Barnes, A., Bullmore, E. T., & Suckling, J. (2009). Endogenous human brain dynamics recover slowly following cognitive effort. *PLoS ONE*, *4*(8). https://doi.org/10.1371/journal.pone.0006626

Bartolomeo, P. (2008). The neural correlates of visual mental imagery: An ongoing debate. *Cortex*, *44*(2), 107–108. https://doi.org/10.1016/j.cortex.2006.07.001

Bartolomeo, P., Hajhajate, D., Liu, J., & Spagna, A. (2020). Assessing the causal role of early visual areas in visual mental imagery. *Nature Reviews Neuroscience*, *21*(9), 517. https://doi.org/10.1038/s41583-020-0348-5

Bassett, D. S., Zurn, P., & Gold, J. I. (2018). On the nature and use of models in network neuroscience. *Nature Reviews Neuroscience*, *19*(9), 566–578. https://doi.org/10.1038/s41583-018-0038-8

Boveroux, P., Vanhaudenhuyse, A., Bruno, M.-A., Noirhomme, Q., Lauwick, S., Luxen, A., Degueldre, C., Plenevaux, A., Schnakers, C., Phillips, C., Brichant, J.-F., Bonhomme, V., Maquet, P., Greicius, M. D., Laureys, S., & Boly, M. (2010). Breakdown of within- and between-network resting state functional magnetic resonance imaging connectivity during propofol-induced loss of consciousness. *Anesthesiology*, *113*(5), 1038–1053. https://doi.org/10.1097/aln.0b013e3181f697f5

Brissenden, J. A., & Somers, D. C. (2019). Cortico–cerebellar networks for visual attention and working memory. *Current Opinion in Psychology*, *29*, 239–247. https://doi.org/10.1016/j.copsyc.2019.05.003

Burt, J. B., Helmer, M., Shinn, M., Anticevic, A., & Murray, J. D. (2020). Generative modeling of Brain Maps with spatial autocorrelation. *NeuroImage*, *220*, 117038. https://doi.org/10.1016/j.neuroimage.2020.117038

Chamberlain, T. A., & Rosenberg, M. D. (2022). Propofol selectively modulates functional connectivity signatures of sustained attention during rest and narrative listening. *Cerebral Cortex*, *32*(23), 5362–5375. https://doi.org/10.1093/cercor/bhac020

Chen, Z., Ivanov, P. C., Hu, K., & Stanley, H. E. (2002). Effect of nonstationarities on Detrended fluctuation analysis. *Physical Review E*, *65*(4). https://doi.org/10.1103/physreve.65.041107

Churchill, N. W., Cimprich, B., Askren, M. K., Reuter-Lorenz, P. A., Jung, M. S., Peltier, S., & Berman, M. G. (2014). Scale-free brain dynamics under physical and psychological distress: Pre-treatment effects in women diagnosed with breast cancer. *Human Brain Mapping*, *36*(3), 1077–1092. https://doi.org/10.1002/hbm.22687

Churchill, N. W., Spring, R., Grady, C., Cimprich, B., Askren, M. K., Reuter-Lorenz, P. A., Jung, M. S., Peltier, S., Strother, S. C., & Berman, M. G. (2016). The suppression of scale-free fmri brain dynamics across three different sources of effort: Aging, Task Novelty and task difficulty. *Scientific Reports*, *6*(1). https://doi.org/10.1038/srep30895

Ciuciu, P., Varoquaux, G., Abry, P., Sadaghiani, S., & Kleinschmidt, A. (2012). Scale-free and multifractal time dynamics of fmri signals during rest and task. *Frontiers in Physiology*, *3*, 1–18. https://doi.org/10.3389/fphys.2012.00186

Clark, S. V., Semmel, E. S., Aleksonis, H. A., Steinberg, S. N., & King, T. Z. (2021). Cerebellar-subcortical-cortical systems as modulators of cognitive functions. *Neuropsychology Review*, *31*(3), 422–446. https://doi.org/10.1007/s11065-020-09465-1

Cocchi, L., Gollo, L. L., Zalesky, A., & Breakspear, M. (2017). Criticality in the brain: A synthesis of neurobiology, models and cognition. *Progress in Neurobiology*, *158*, 132–152. https://doi.org/10.1016/j.pneurobio.2017.07.002

Davis, M. H., Coleman, M. R., Absalom, A. R., Rodd, J. M., Johnsrude, I. S., Matta, B. F., Owen, A. M., & Menon, D. K. (2007). Dissociating speech perception and comprehension at reduced levels of awareness. *Proceedings of the National Academy of Sciences*, *104*(41), 16032–16037. https://doi.org/10.1073/pnas.0701309104

Dueck, M. H., Petzke, F., Gerbershagen, H. J., Paul, M., Hesselmann, V., Girnus, R., Krug, B., Sorger, B., Goebel, R., Lehrke, R., Sturm, V., & Boerner, U. (2005). Propofol attenuates responses of the auditory cortex to acoustic stimulation in a dose-dependent manner: A FMRI study. *Acta Anaesthesiologica Scandinavica*, *49*(6), 784–791. https://doi.org/10.1111/j.1399-6576.2005.00703.x

Eagleman, S. L., Chander, D., Reynolds, C., Ouellette, N. T., & MacIver, M. B. (2019). Complexity measures of the electroencephalograph capture loss and recovery of consciousness in patients anesthetized with propofol. *BioRxiv*. https://doi.org/10.1101/594002

Ferrarelli, F., Massimini, M., Sarasso, S., Casali, A., Riedner, B. A., Angelini, G., Tononi, G., & Pearce, R. A. (2010). Breakdown in cortical effective connectivity during midazolam-induced loss of consciousness. *Proceedings of the National Academy of Sciences*, *107*(6), 2681–2686. https://doi.org/10.1073/pnas.0913008107

Franks, N. P., & Wisden, W. (2021). The inescapable drive to sleep: Overlapping mechanisms of sleep and sedation. *Science*, *374*(6567), 556–559. https://doi.org/10.1126/science.abi8372

Galaska, R., Makowiec, D., Dudkowska, A., Koprowski, A., Chlebus, K., Wdowczyk-Szulc, J., & Rynkiewicz, A. (2008). Comparison of wavelet transform modulus maxima and

multifractal detrended fluctuation analysis of heart rate in patients with systolic dysfunction of left ventricle. *Annals of Noninvasive Electrocardiology*, *13*(2), 155–164. https://doi.org/10.1111/j.1542-474x.2008.00215.x

Ganis, G., Thompson, W. L., & Kosslyn, S. M. (2004). Brain areas underlying visual mental imagery and visual perception: An fmri study. *Cognitive Brain Research*, *20*(2), 226–241. https://doi.org/10.1016/j.cogbrainres.2004.02.012

Gross, W. L., Lauer, K. K., Liu, X., Roberts, C. J., Liu, S., Gollapudy, S., Binder, J. R., Li, S.-J., & Hudetz, A. G. (2019). Propofol sedation alters perceptual and cognitive functions in healthy volunteers as revealed by Functional Magnetic Resonance Imaging. *Anesthesiology*, *131*(2), 254–265. https://doi.org/10.1097/aln.0000000000002669

Hall, T. M., de Carvalho, F., & Jackson, A. (2014). A common structure underlies low-frequency cortical dynamics in movement, sleep, and Sedation. *Neuron*, *83*(5), 1185–1199. https://doi.org/10.1016/j.neuron.2014.07.022

Hamaguchi, K., Kato, K., Kubo, T., Uesugi, F., Hidaka, S., & Nakagawa, I. (2005). Effect of propofol on visual evoked potentials during neurosurgery. *The Japanese Journal of Anesthesiology*, *54*(9), 998–1002.

He, B. J. (2011). Scale-free properties of the functional magnetic resonance imaging signal during rest and task. *The Journal of Neuroscience*, *31*(39), 13786–13795. https://doi.org/10.1523/jneurosci.2111-11.2011

Huang, Z., Vlisides, P. E., Tarnal, V. C., Janke, E. L., Keefe, K. M., Collins, M. M., McKinney, A. M., Picton, P., Harris, R. E., Mashour, G. A., & Hudetz, A. G. (2018). Brain imaging reveals covert consciousness during behavioral unresponsiveness induced by propofol. *Scientific Reports*, *8*(1). https://doi.org/10.1038/s41598-018-31436-z

Hudetz, A. G. (2012). General anesthesia and human brain connectivity. *Brain Connectivity*, *2*(6), 291–302. https://doi.org/10.1089/brain.2012.0107

Hudetz, A. G., & Imas, O. A. (2007). Burst activation of the cerebral cortex by flash stimuli during isoflurane anesthesia in rats. *Anesthesiology*, *107*(6), 983–991. https://doi.org/10.1097/01.anes.0000291471.80659.55

Hurst, H. E. (1951). Long-term storage capacity of reservoirs. *Transactions of the American Society of Civil Engineers*, *116*(1), 770–799. https://doi.org/10.1061/taceat.0006518

Kandeepan, S., Rudas, J., Gomez, F., Stojanoski, B., Valluri, S., Owen, A. M., Naci, L., Nichols, E. S., & Soddu, A. (2020). Modeling an auditory stimulated brain under altered states of consciousness using the generalized Ising model. *NeuroImage*, *223*, 117367. https://doi.org/10.1016/j.neuroimage.2020.117367

Kantelhardt, J. W., Zschiegner, S. A., Koscielny-Bunde, E., Havlin, S., Bunde, A., & Stanley, H. E. (2002). Multifractal detrended fluctuation analysis of Nonstationary Time Series. *Physica A: Statistical Mechanics and Its Applications*, *316*(1-4), 87–114. https://doi.org/10.1016/s0378-4371(02)01383-3

Kardan, O., Adam, K. C. S., Mance, I., Churchill, N. W., Vogel, E. K., & Berman, M. G. (2020). Distinguishing cognitive effort and working memory load using scale-invariance and alpha suppression in EEG. *NeuroImage*, *211*, 116622. https://doi.org/10.1016/j.neuroimage.2020.116622

Kardan, O., Layden, E., Choe, K. W., Lyu, M., Zhang, X., Beilock, S. L., Rosenberg, M. D., & Berman, M. G. (2020). Scale-invariance in brain activity predicts practice effects in cognitive performance. *BioRxiv*. https://doi.org/10.1101/2020.05.25.114959

Kim, K. M., Jeon, W. J., Lee, D. H., Kang, W. C., Kim, J. H., & Noh, G. J. (2004). Changes in visual and auditory response time during conscious sedation with propofol. *Acta Anaesthesiologica Scandinavica*, *48*(8), 1033–1037. https://doi.org/10.1111/j.0001-5172.2004.00469.x

Kosslyn, S. M., Ganis, G., & Thompson, W. L. (2001). Neural Foundations of Imagery. *Nature Reviews Neuroscience*, *2*(9), 635–642. https://doi.org/10.1038/35090055

Kosslyn, S. M., Pascual-Leone, A., Felician, O., Camposano, S., Keenan, J. P., L., W., Thompson, Ganis, G., Sukel, K. E., & Alpert, N. M. (1999). The role of area 17 in visual imagery: Convergent evidence from pet and RTMS. *Science*, *284*(5411), 167–170. https://doi.org/10.1126/science.284.5411.167

Lee, J.-M., Kim, D.-J., Kim, I.-Y., Park, K.-S., & Kim, S. I. (2002). Detrended fluctuation analysis of EEG in sleep apnea using MIT/BiH polysomnography data. *Computers in Biology and Medicine*, *32*(1), 37–47. https://doi.org/10.1016/s0010-4825(01)00031-2

Liu, X., Lauer, K. K., Ward, B. D., Rao, S. M., Li, S.-J., & Hudetz, A. G. (2012). Propofol disrupts functional interactions between sensory and high-order processing of auditory verbal memory. *Human Brain Mapping*, *33*(10), 2487–2498. https://doi.org/10.1002/hbm.21385

Luppi, A. I., Craig, M. M., Pappas, I., Finoia, P., Williams, G. B., Allanson, J., Pickard, J. D., Owen, A. M., Naci, L., Menon, D. K., & Stamatakis, E. A. (2019). Consciousness-specific dynamic interactions of brain integration and functional diversity. *Nature Communications*, *10*(1). https://doi.org/10.1038/s41467-019-12658-9

López, J. L., Hernández, S., Urrutia, A., López-Cortés, X. A., Araya, H., & Morales-Salinas, L. (2021). Effect of missing data on short time series and their application in the characterization of surface temperature by detrended fluctuation analysis. *Computers & Geosciences*, *153*, 104794. https://doi.org/10.1016/j.cageo.2021.104794

Maksimow, A., Silfverhuth, M., Långsjö, J., Kaskinoro, K., Georgiadis, S., Jääskeläinen, S., & Scheinin, H. (2014). Directional connectivity between frontal and posterior brain regions is altered with increasing concentrations of propofol. *PLoS ONE*, *9*(11). https://doi.org/10.1371/journal.pone.0113616

Markett, S., Reuter, M., Montag, C., Voigt, G., Lachmann, B., Rudorf, S., Elger, C. E., & Weber, B. (2013). Assessing the function of the Fronto-parietal attention network: Insights from resting-state fmri and the Attentional Network Test. *Human Brain Mapping*, *35*(4), 1700–1709. https://doi.org/10.1002/hbm.22285

Monti, M. M., Vanhaudenhuyse, A., Coleman, M. R., Boly, M., Pickard, J. D., Tshibanda, L., Owen, A. M., & Laureys, S. (2010). Willful modulation of brain activity in disorders of consciousness. *New England Journal of Medicine*, *362*(7), 579–589. https://doi.org/10.1056/nejmoa0905370

Moro, V., Berlucchi, G., Lerch, J., Tomaiuolo, F., & Aglioti, S. M. (2008). Selective deficit of mental visual imagery with intact primary visual cortex and visual perception. *Cortex*, *44*(2), 109–118. https://doi.org/10.1016/j.cortex.2006.06.004

Motzkin, J. C., Baskin-Sommers, A., Newman, J. P., Kiehl, K. A., & Koenigs, M. (2014). Neural correlates of substance abuse: Reduced functional connectivity between areas underlying reward and cognitive control. *Human Brain Mapping*, *35*(9), 4282–4292. https://doi.org/10.1002/hbm.22474

Naci, L., Haugg, A., MacDonald, A., Anello, M., Houldin, E., Naqshbandi, S., Gonzalez-Lara, L. E., Arango, M., Harle, C., Cusack, R., & Owen, A. M. (2018). Functional diversity of brain networks supports consciousness and verbal intelligence. *Scientific Reports*, *8*(1). https://doi.org/10.1038/s41598-018-31525-z

Oświęcimka, P., Kwapień, J., & Drożdż, S. (2006). Wavelet versus detrended fluctuation analysis of multifractal structures. *Physical Review E*, *74*(1). https://doi.org/10.1103/physreve.74.016103

Pearson, J., Naselaris, T., Holmes, E. A., & Kosslyn, S. M. (2015). Mental imagery: Functional mechanisms and clinical applications. *Trends in Cognitive Sciences*, *19*(10), 590–602. https://doi.org/10.1016/j.tics.2015.08.003

Peng, C. K., Havlin, S., Stanley, H. E., & Goldberger, A. L. (1995). Quantification of scaling exponents and crossover phenomena in nonstationary heartbeat time series. *Chaos: An Interdisciplinary Journal of Nonlinear Science*, *5*(1), 82–87. https://doi.org/10.1063/1.166141

Plourde, G., Belin, P., Chartrand, D., Fiset, P., Backman, S. B., Xie, G., & Zatorre, R. J. (2006). Cortical processing of complex auditory stimuli during alterations of consciousness with the general anesthetic propofol. *Anesthesiology*, *104*(3), 448–457. https://doi.org/10.1097/00000542-200603000-00011

Rhif, M., Ben Abbes, A., Farah, I., Martínez, B., & Sang, Y. (2019). Wavelet transform application for/in Non-Stationary Time-Series Analysis: A Review. *Applied Sciences*, *9*(7), 1345. https://doi.org/10.3390/app9071345

Shen, X., Tokoglu, F., Papademetris, X., & Constable, R. T. (2013). Groupwise whole-brain parcellation from resting-state fmri data for network node identification. *NeuroImage*, *82*, 403–415. https://doi.org/10.1016/j.neuroimage.2013.05.081

Song, I. H., Ji, Y. S., Cho, B. K., Ku, J. H., Chee, Y. J., Lee, J. S., Lee, S. M., Kim, I. Y., & Kim, S. I. (2007). Multifractal analysis of sleep EEG dynamics in humans. *2007 3rd International IEEE/EMBS Conference on Neural Engineering*, 546–549. https://doi.org/10.1109/cne.2007.369730

Spagna, A., Hajhajate, D., Liu, J., & Bartolomeo, P. (2020). Visual mental imagery engages the left fusiform gyrus, but not the early visual cortex: A meta-analysis of neuroimaging evidence. https://doi.org/10.1101/2020.02.06.937151

Sriraam, N., Purnima, B. R., Uma, K., & Padmashri, T. K. (2014). Hurst exponents based detection of wake-sleep - a pilot study. *International Conference on Circuits, Communication, Control and Computing*, 118–121. https://doi.org/10.1109/cimca.2014.7057771

Stier, A. J., Cardenas-Iniguez, C., Kardan, O., Moore, T. M., Meyer, F. A., Rosenberg, M. D., Kaczkurkin, A. N., Lahey, B. B., & Berman, M. G. (2021). A scale-free gradient of Cognitive Resource Disruptions In Childhood psychopathology. *BioRxiv*. https://doi.org/10.1101/2021.08.24.457554

Tarvainen, M. P., Georgiadis, S., Laitio, T., Lipponen, J. A., Karjalainen, P. A., Kaskinoro, K., & Scheinin, H. (2012). Heart rate variability dynamics during low-dose propofol and dexmedetomidine anesthesia. *Annals of Biomedical Engineering*, *40*(8), 1802–1813. https://doi.org/10.1007/s10439-012-0544-1

Tobias, J. D., & Leder, M. (2011). Procedural sedation: A review of Sedative Agents, monitoring, and management of complications. *Saudi Journal of Anaesthesia*, *5*(4), 395. https://doi.org/10.4103/1658-354x.87270

Varley, T. F., Luppi, A. I., Pappas, I., Naci, L., Adapa, R., Owen, A. M., Menon, D. K., & Stamatakis, E. A. (2020). Consciousness & Brain functional complexity in propofol anaesthesia. *Scientific Reports*, *10*(1). https://doi.org/10.1038/s41598-020-57695-3

Veselis, R. A., Reinsel, R. A., Wronski, M., Marino, P., Tong, W. P., & Bedford, R. F. (1992). EEG and memory effects of low-dose infusions of propofol . *British Journal of Anaesthesia*, *69*(3), 246–254. https://doi.org/10.1093/bja/69.3.246

Veselis, R. A., Reinsel, R. A., Wronski, M., Marino, P., Tong, W. P., & Bedford, R. F. (1992). EEG and memory effects of low-dose infusions of propofol. *British Journal of Anaesthesia*, *69*(3), 246–254. https://doi.org/10.1093/bja/69.3.246

Vincent, J. L., Kahn, I., Snyder, A. Z., Raichle, M. E., & Buckner, R. L. (2008). Evidence for a frontoparietal control system revealed by intrinsic functional connectivity. *Journal of Neurophysiology*, *100*(6), 3328–3342. https://doi.org/10.1152/jn.90355.2008

Wang, L., Liu, X., Guise, K. G., Knight, R. T., Ghajar, J., & Fan, J. (2010). Effective connectivity of the Fronto-parietal network during attentional control. *Journal of Cognitive Neuroscience*, *22*(3), 543–553. https://doi.org/10.1162/jocn.2009.21210

Wei, M., Qin, J., Yan, R., Li, H., Yao, Z., & Lu, Q. (2013). Identifying major depressive disorder using Hurst exponent of resting-state brain networks. *Psychiatry Research: Neuroimaging*, *214*(3), 306–312. https://doi.org/10.1016/j.pscychresns.2013.09.008

Wendt, H., Abry, P., & Jaffard, S. (2007). Bootstrap for empirical multifractal analysis. *IEEE Signal Processing Magazine*, *24*(4), 38–48. https://doi.org/10.1109/msp.2007.4286563

White, N. S., & Alkire, M. T. (2003). Impaired thalamocortical connectivity in humans during general-anesthetic-induced unconsciousness. *NeuroImage*, *19*(2), 402–411. https://doi.org/10.1016/s1053-8119(03)00103-4

Won, D.-O., Lee, B.-R., Seo, K.-S., Kim, H. J., & Lee, S.-W. (2019). Alteration of coupling between brain and heart induced by sedation with propofol and Midazolam. *PLoS ONE*, *14*(7). https://doi.org/10.1371/journal.pone.0219238

Zhuang, C., Meidenbauer, K. L., Kardan, O., Stier, A. J., Choe, K. W., Cardenas-Iniguez, C., Huppert, T. J., & Berman, M. G. (2022). Scale invariance in fNIRS as a measurement of cognitive load. *Cortex*, *154*, 62–76. https://doi.org/10.1016/j.cortex.2022.05.009

Zorick, T., & Mandelkern, M. A. (2013). Multifractal detrended fluctuation analysis of human EEG: Preliminary investigation and comparison with the wavelet transform modulus maxima technique. *PLoS ONE*, *8*(7). https://doi.org/10.1371/journal.pone.0068360

Appendix

Supplementary Figure 1

R-squared distribution for DFA-based H

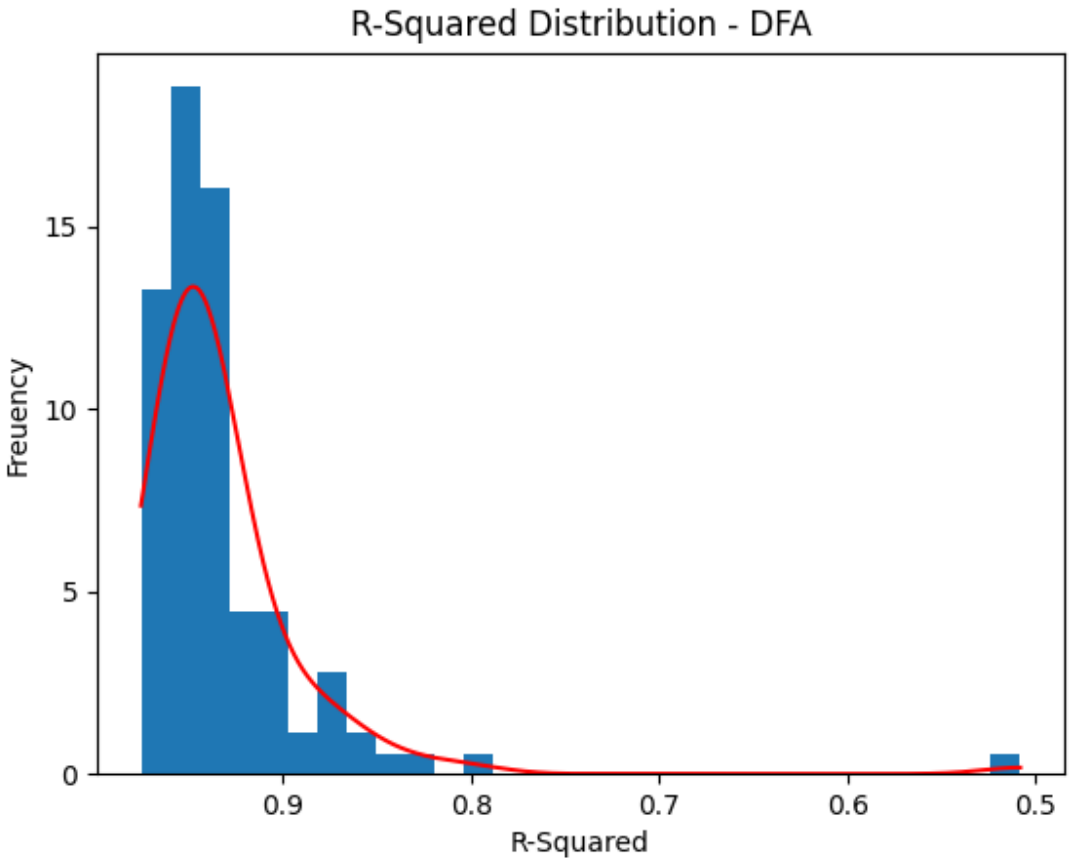

Note. The distribution of the R^2 values obtained from the DFA analysis is presented in this figure. Overall, the goodness of fit is quite high, with the majority of values having a mean R^2 exceeding 0.9. These findings further validate our choice to utilize DFA results for subsequent analyses.

Supplementary Figure 2

PLS results for the resting state condition

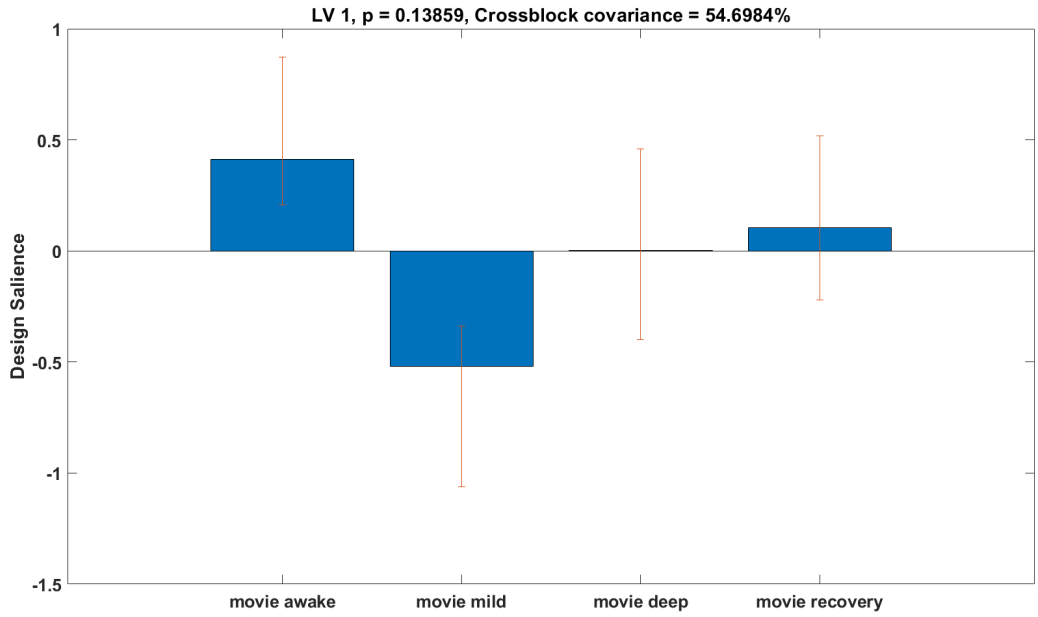

Note. Although the trend of *H* in the rest condition exhibited an opposite pattern compared to the narrative listening condition, caution should be exercised in interpreting these non-significant findings, particularly given the relatively small sample size. Over-interpretation of non-significant results can lead to erroneous conclusions and detract from the rigor of the study.

Supplementary Figure 3

PLS results with eight scanning sessions

(a)

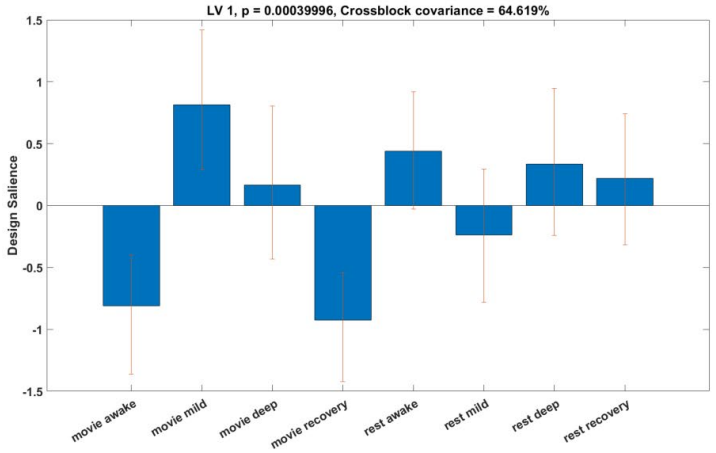

(b)

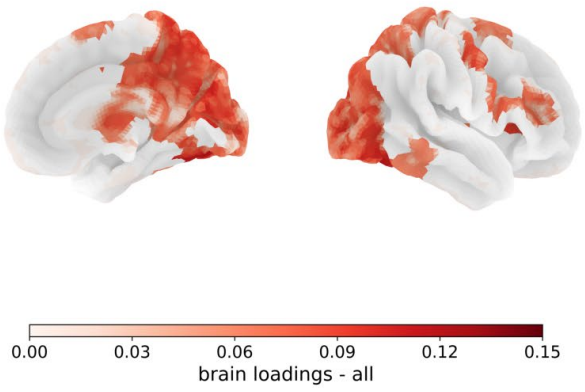

Note. (a) The PLS results containing all eight scanning sessions (2 condition × 4 sedation levels) revealed one single latent variable ($p < 0.001$, crossblock covariance = 64.619%); (b) The plotting of significantly stable brain nodes in this PLS model revealed a pattern that closely resembled the separate narrative listening model, with a majority of significant brain nodes clustering around the occipitoparietal cortex and motor areas.

Supplementary Figure 4

Neurosynth template for visual attention and stress

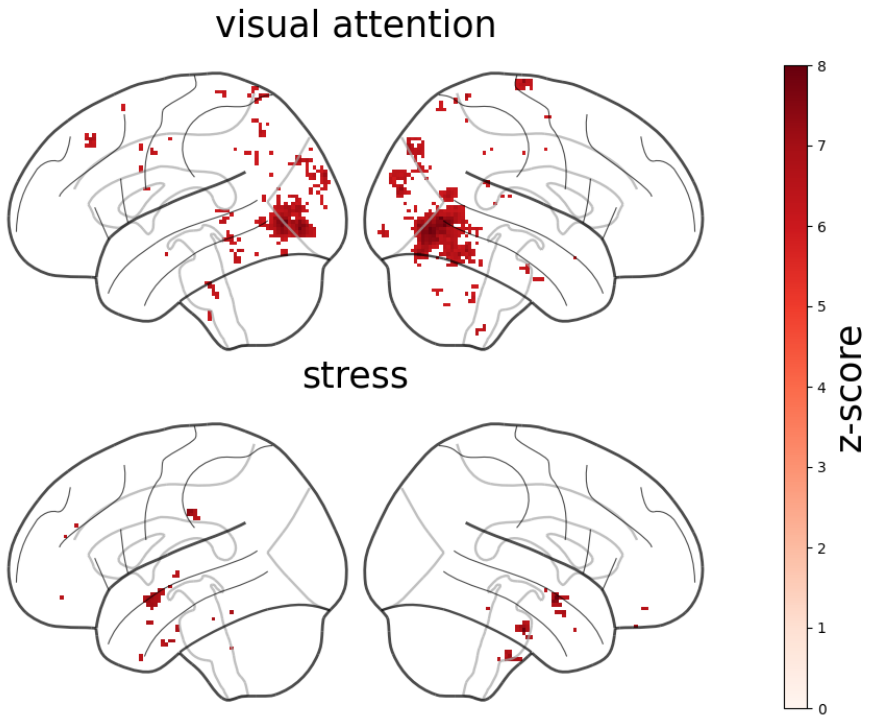

Note. This figure depicts the original association map for visual attention and stress. Notably, the visual attention map exhibits significant overlap with the spatial pattern generated from our PLS model, particularly in the bilateral occipitoparietal areas. Conversely, the stress map reveals activations in the temporal areas which were largely insignificant in our model after ruling out unstable brain loadings.

Supplementary Figure 5

Left brain maps for early versus late models

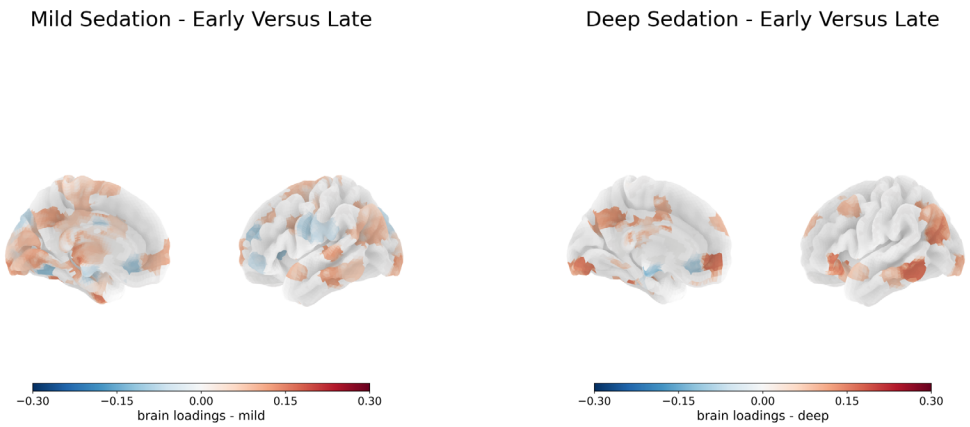

Note. This figure is a supplement to the bottom panel of *Figure 12* and displays the left hemisphere in the PLS models for the early and late scanning session periods in both mild and deep sedation conditions.